Research Square

Preprints are preliminary reports that have not undergone peer review.
They should not be considered conclusive, used to inform clinical practice,
or referenced by the media as validated information.

Single-cell entropy as a selectable and inducible marker of stem-cell youth: a multi-track technical architecture for producing young autologous hematopoietic stem cells

Jaba Tqemaladze

djabbat@gmail.com

Universidad a Distancia de Madrid https://orcid.org/0000-0001-8651-7243

Research Article

Keywords: stem-cell ageing, single-cell entropy, haematopoietic stem cells, autologous cell therapy, reprogramming, centriole, meiotic recombination, totipotency, niche rejuvenation

Posted Date: October 6th, 2026

DOI: https://doi.org/10.21203/rs.3.rs-11245878/v1

License: This work is licensed under a Creative Commons Attribution 4.0 International License.
Read Full License

Additional Declarations: The authors declare no competing interests.

Single-cell entropy as a selectable and inducible marker of stem-cell youth: a multi-track technical architecture for producing young autologous hematopoietic stem cells

Jaba Tqemaladze 1,2

1 PhD Programme 9620, Universidad Nacional de Educación a Distancia (UNED), Madrid, Spain 2 Georgia Longevity Alliance, Tbilisi, Georgia

ORCID: 0000-0001-8651-7243 | **Correspondence:** jaba@longevity.ge

Manuscript type: Registered Report — Stage 1 (hypothesis and protocol; no primary data). Submitted for in-principle acceptance under the two-stage Registered Report model; Stage 2 adds data and results without modifying the hypotheses or the analysis plan.

Word count (main text): ~12,800 | **Figures:** 1 (architecture) | **Tables:** 8 | **References:** 70

Abstract

Background. Ageing of the haematopoietic system is driven, at the stem-cell level, by the accumulation of functionally compromised stem cells in the bone-marrow niche. Age-associated single-cell entropy (the loss of transcriptomic coordination within a cell of a given type) is computable from single-cell transcriptomic and chromatin data, increases with age, and has never been used as a *selectable and inducible* property to obtain young autologous adult stem cells. **Objectives.** We formalise a falsifiable research programme and a complete technical architecture for producing young, safe, autologous adult HSCs whose age-associated single-cell entropy is lower than that of the corresponding cells in vivo, that engraft in the niche without pharmacological immunosuppression, subject to a mitochondrial-neoantigen screen, and that replace aged cells with functional young progeny. Track R and Track C are presented as gated, exploratory directions outside the registered dataset; the registered core is Track A and Track T1. **Architecture.** Five coordinated tracks share a set of technical nodes. A cross-cutting preparation layer (LERR, ladders L1–L5) stages and readiness-gates autologous cells. Track A measures single-cell entropy across division history and donor age, tests the division-rate–entropy coupling, and selects or induces low-entropy cells. Track R reverse-engineers the natural reproductive entropy partition: somatic-to-germline induction (PGCLC), induced meiosis, blockade of meiotic recombination for isogenicity, haploid stabilisation, gamete fusion, zygotic genome activation, and

totipotency induction. Track C safely eliminates the centriole while preserving diploidy, inducing totipotency and direct differentiation without an embryo. Track T1 rejuvenates resident HSCs in situ by senolytic niche clearance and niche-signal restoration. The tracks share six identical procedures (totipotency induction, single-cell entropy verification, differentiation-inductor delivery, de-novo centriole biogenesis, genome-integrity gating, niche engraftment), which consolidate the experimental programme into a single coordinated pipeline. **Hypotheses.** Eleven falsifiable hypotheses (H1–H5 with sub-hypotheses H4b–H4g) are pre-registered with explicit falsification criteria; automation (H6) is an engineering acceptance criterion rather than a biological hypothesis and is excluded from the hypothesis count and from multiple-comparison control; genome integrity and tumorigenicity are co-primary safety gates for every track. **Conclusions.** A systematic search of the literature returns no direct test of entropy-selected autologous niche replacement, which we propose as the central, addressable gap. Each node is expressed as a measurable operation with a defined failure condition, negative results surface at the node where evidence is missing, and the programme is therefore suited to staged, high-risk/high-reward evaluation.

Keywords: stem-cell ageing; single-cell entropy; haematopoietic stem cells; autologous cell therapy; reprogramming; centriole; meiotic recombination; totipotency; niche rejuvenation

Significance statement. Ageing of the blood system is driven by aged stem cells accumulating in the marrow. We propose that age-associated single-cell entropy (the loss of transcriptomic coordination in an individual stem cell of its type) can be selected and induced, and that returning the patient's own low-entropy cells to the niche can replace aged blood production without allogeneic immune barriers. The paper formalises a falsifiable, five-track technical architecture in which every operation is expressed as a measurable procedure with a defined failure condition, and grades the published evidence for every node.

1. Introduction

1.1 Ageing of the haematopoietic system as a stem-cell problem

The haematopoietic compartment is maintained for a lifetime by a small pool of HSCs whose self-renewal and differentiation output must remain balanced. With age this balance is lost. Published work on both mice and humans shows that aged HSCs accumulate in the bone-marrow niche with reduced self-renewal, skewed and biased lineage output (most prominently toward myeloid and away from lymphoid fates), increased DNA damage, and progressive epigenetic drift (Rossi et al., 2005; Dykstra et al., 2011). Clonal analyses demonstrate that the functional decline is cell-intrinsic and heterogeneous across the HSC pool rather than a uniform property of the whole

population (Dykstra et al., 2011). The practical consequence is a measurable decline in the adaptive immune repertoire, in haematopoietic reserve after stress, and in the capacity to repopulate a transplanted host — a decline that tracks donor chronological age only loosely.

Two features of this system make it an unusually tractable model for a first test of stem-cell rejuvenation. First, HSCs are autologous and minimally invasive to obtain (peripheral blood mobilisation or bone-marrow aspiration), so a cell product made from a patient's own cells faces no fundamental immune-barrier problem. Second, HSCs are single-cell resolvable: their transcriptome and open-chromatin landscape can be measured one cell at a time, which is precisely the resolution at which an ageing state must be defined and, in principle, sorted.

1.2 Single-cell entropy: a computable, cell-intrinsic ageing metric

A single cell's regulatory state can be summarised as an entropy-like quantity. The signalling-entropy formalism computes, for each cell, the Shannon entropy of the probability distribution over the cell's signalling-network nodes derived from its transcriptome, and has been shown to correlate with differentiation potency and developmental potential without any trained model (Teschendorff & Enver, 2017). Independently, cell-type-specific ageing clocks built from single-cell data quantify ageing and rejuvenation within defined cell types (Buckley et al., 2023), and single-cell RNA-seq has resolved age-associated changes in the cell-cycle and differentiation programs of HSCs themselves (Kowalczyk et al., 2015). These two lines of evidence establish that (i) single-cell entropy is computable from routine single-cell assays, and (ii) it carries information about both potency and age at the level of the individual cell.

Three properties make single-cell entropy more attractive than chronological age as a marker of stem-cell state. It is cell-intrinsic rather than a population statistic; it integrates replicative history, epigenetic drift, and molecular damage into a single number; and (unlike "age") it is in principle selectable, because a cell can be measured and then physically sorted on the basis of its value. This last property is the point of departure of the present programme: the programme uses entropy as a property to be selected and, where selection is insufficient, to be induced, rather than as a biomarker to be read.

1.2a Two distinct entropy directions must not be conflated

"Entropy" in single-cell biology denotes two different quantities, and the distinction is decisive for this programme. First, signalling entropy (Teschendorff & Enver, 2017) measures differentiation potency: it is high in pluripotent and undifferentiated cells and low in terminally differentiated cells. Second, age-associated entropy denotes the loss of transcriptomic coordination within a cell of a fixed type, measured as the deviation of a cell's expression state from a well-ordered type-specific reference; it increases with

age and correlates with mitotic age (Buckley et al., 2023; Yang et al., 2026). These two quantities run in opposite directions across potency, so they cannot be treated as one readout.

The selection logic of this programme applies strictly to age-associated entropy measured *within the HSC compartment*: one HSC is compared with another HSC of the same cell type, never with its progeny. A low age-associated-entropy HSC is one whose transcriptional program is tightly coordinated for its type, not one with low differentiation potency. Signalling (potency) entropy is therefore not used as the selection criterion; where it is reported at all, it is flagged as a potency measure and analysed separately. This distinction removes an apparent contradiction: selecting the lowest age-associated-entropy fraction selects the most youth-like HSCs, not the least potent ones.

1.3 The central gap: age-associated entropy has never been used as a selectable and inducible property for autologous stem-cell return

A systematic search of PubMed and preprint servers (E-utilities, 2026-09-20 and 2026-10-02; full strategy in Appendix A) with the queries *single-cell entropy AND stem cell AND rejuvenation*, *entropy AND autologous AND hematopoietic stem cell AND selection*, and *division rate AND single-cell entropy* returned no study that selects low-entropy autologous adult stem cells by single-cell entropy and returns them to the niche with functional engraftment testing. The immediate conceptual neighbourhood is active rather than empty: a 2026 preprint quantifies transcriptional entropy as deviation from a transcriptomic manifold, shows that it increases with age and correlates with chromatin-based mitotic age, and identifies regenerative compartments including haematopoiesis as most affected (Yang et al., 2026); cell-type-specific ageing clocks already resolve age within defined cell types (Buckley et al., 2023); a 2025 preprint uses deep learning on 3D chromatin images to predict HSC ageing and explicitly treats chromatin entropy as a predictive marker (Iáñez Picazo et al., 2025); and a 2026 preprint reports a large multi-omics atlas of human HSPC ageing (> 380,000 paired RNA/ATAC profiles, 77 donors) showing increased cis-regulatory entropy with age (Stevens et al., 2026). A further prior must be acknowledged: a 2022 study maps Shannon entropy across human haematopoietic differentiation, showing a transient entropy peak at single-cell level and elevated entropy in the immature compartment of myelodysplastic syndromes (Dussiau et al., 2022); that work concerns differentiation-potency entropy rather than age-associated disorder and does not select cells for autologous return, but it is part of the conceptual neighbourhood and is therefore acknowledged here rather than excluded by a narrow query. That atlas and these priors are descriptive — they document that entropy varies with differentiation and age — whereas the present programme is operational: it uses transcriptomic age-associated entropy as a selectable and inducible property in an autologous return protocol. The descriptive works are references for the present coupling and selection claims, not prior tests of them. What

none of these does is use *transcriptomic* age-associated entropy as a selectable and inducible property in an autologous niche-replacement procedure. Direct tests of a division-rate–entropy coupling in HSCs were likewise absent at the time of search. Partial reprogramming in vivo and ex vivo demonstrably improves markers of ageing (Ocampo et al., 2016; Lu et al., 2020; Sahu et al., 2024), but the published readouts are bulk or population-level; none uses single-cell age-associated entropy as the quantified, selectable endpoint of a rejuvenation protocol.

The scientific contribution of the programme is defined by this gap. It is a hypothesis-driven research architecture: the constituent operations are individually plausible on current evidence, but their integration (selection, induction, and autologous return of low-entropy adult stem cells) is untested, and each step is therefore expressed as a falsifiable hypothesis with a defined failure condition. The programme advances three claims that no published study has tested: (1) transcriptomic age-associated entropy is a selectable property of adult stem cells, not merely a population-level biomarker; (2) a low-entropy state can be induced where selection is insufficient, with entropy as the quantified endpoint; and (3) autologous low-entropy cells returned to the niche can replace aged haematopoiesis without immunosuppression. Claims (1) and (3) are tested by H1–H4, claim (2) by H4b–H4g.

1.4 Red thread

The organism ages because aged stem cells with high age-associated entropy accumulate in their niches; their division tempo falls, niche-signal perception and self-renewal decline, and tissue self-repair declines relative to self-destruction. Single-cell entropy is a measurable, selectable proxy of this ageing state, and is plausibly coupled to division rate. Selecting low-entropy autologous cells and returning them to the niche should replace aged cells without allogeneic rejection, because the returned cells are the patient's own; the claim is conditional on the product passing the immunogenicity screen of Section 11. Where selection yields too few young cells, a low-entropy state is induced rather than harvested. The deepest form of induction reproduces the one mechanism by which nature reliably produces a young cell: the partitioning of entropy that occurs at reproduction — gamete production, meiosis, and the epigenetic reset of the fertilised egg.

1.5 A note on the conceptual lineage

The programme is an extension of a line of work on cell division and ageing that connects the centriole to differentiation and replicative ageing: the proposal that the centriole determines the morphogenetic status of somatic cells (Tkemaladze & Chichinadze, 2005a), its extension to centriolar mechanisms of differentiation and replicative ageing (Tkemaladze & Chichinadze, 2005b), the centriole–differentiation–senescence link (Tkemaladze & Chichinadze, 2010), and the proposal that selective

accumulation of old centrioles underlies stem-cell division defects (Tkemaladze, 2023). All four are the author's own work, all are PubMed-indexed with PMIDs, and none is independently verified. The premise that stem cells track their division history is not unique to this lineage: it is independently documented in HSCs, which count and remember self-renewal divisions (Bernitz et al., 2016). The centriole-division-counter model is a hypothesis and has not been independently verified; it is not a prerequisite of this architecture: the entropy-selection track (Track A) and the in-situ track (Track T1) are entirely independent of centriole manipulation, and the centriole-dependent tracks (R, C) are presented as explicitly speculative, falsifiable alternatives with hard feasibility gates. The manuscript does not claim the model as an established driver of HSC ageing; it is used only where a centriole-based route is being tested on its own terms.

1.6 Structure of the paper

Section 2 states the eleven pre-registered hypotheses and their falsification criteria. Section 3 lays out the multi-track architecture and its shared nodes. Section 4 specifies the cross-cutting preparation layer (LERR). Sections 5–8 detail the four tracks (A, R, C, T1) node by node, with rationale, procedure, and failure condition for each; Section 5.7 contains the full executable pilot protocol for the primary arm. Section 9 consolidates the shared nodes, Section 10 specifies the single-cell entropy methodology, Section 11 the safety gate, and Section 12 the statistical design, decision gates, and reporting. Section 13 discusses weaknesses, assesses the evidence for every node, and answers the strongest counterarguments. Section 14 concludes. Sections 13–14 are interpretive context retained for this preprint; the Stage 1 journal submission package follows the target journal's structure (Introduction, Methods including the analysis plan, and pilot plan), and the discussion and conclusions are relocated to Stage 2 or to supplementary material as the journal requires. The journal Stage 1 submission will be condensed to the target journal's word limit (typically 5,000–8,000 words for Nature-series Registered Reports), with the architecture compressed and operational detail moved to supplementary; this preprint retains the full architecture for completeness. The full executable protocol for Section 5.7 is available as a companion methods document (Tqemaladze, 2026, *Protocol: division tracking, index sorting, and single-cell entropy in human HSCs*); this Article retains only the decision-relevant parameters and references the companion for operational detail.

2. Pre-registered, falsifiable hypotheses

Each hypothesis is stated with its falsification criterion. Evidence levels are [E] established, [I] inferred, [H] hypothetical, [P] pre-registered to be tested.

H1 (Coupling) [P]: In human HSCs, division history and age-associated single-cell entropy (transcriptional disorder within the HSC type) are positively associated: cells

that have divided more, or divided aberrantly, show higher age-associated entropy. *Falsified if* the association is not statistically significant after controlling for cell-cycle state and donor age. Additionally, the magnitude is reported against a pre-specified interpretive threshold (SESOI = $|\beta| \geq 0.1$ SD units of entropy per division, with the 95% confidence-interval lower bound above 0.05 SD units), which is set by convention from the Cohen small-effect benchmark rather than from domain-specific evidence (none exists); effects that are statistically significant but below this threshold are reported as significant yet below the interpretive threshold and are not counted as confirmation of a biologically relevant coupling. Functional anchoring: in the Objective 1 atlas, age-associated entropy and at least one functional readout (lineage-bias index; serial-transplantation capacity where the engraftment arm allows) are measured on the same donors, and the ratio of the entropy-division slope to the functional-division slope is reported; a coupling that is statistically significant but whose functional-division slope is indistinguishable from zero is reported as existing without demonstrated functional meaning and does not by itself justify the selection rationale.

H2 (Selectability) [P]: An age-associated-entropy signature, translated into a surface-marker proxy or an index-based selection rule derived from the Objective 1 atlas, can identify an HSC fraction that is measurably lower in age-associated entropy than age-matched, donor-matched in-vivo HSCs of the same cell type. The claim is not tautological: the proxy (markers or index rule) is fixed before sorting, so the question is whether the proxy recovers the low-entropy state rather than whether “the lowest-entropy cells have low entropy”, which would be true by definition. *Falsified if* the fraction recovered by the pre-fixed proxy is not significantly lower in age-associated entropy than its in-vivo counterpart.

H3 (No rejection) [P]: Autologous low-entropy HSCs returned to the bone-marrow niche engraft without immunosuppression and without immune rejection, and are functionally equivalent or superior to unselected autologous HSCs. Engraftment is defined operationally as donor-derived multilineage chimerism above a pre-specified threshold (≥ 1% human CD45+ cells and ≥ 1% per major lineage at 16 weeks), a criterion consistent with published humanised-mouse HSC engraftment studies (Hasgur et al., 2016), and rejection as failure to maintain that chimerism with no detectable anti-donor response. *Falsified if* autologous engraftment fails to reach the chimerism threshold, requires immunosuppression, or is accompanied by an immune response against the returned cells. In the pilot, the engraftment arm ($n = 8$ per arm) is a feasibility endpoint: it has only approximately 40% power to detect a doubling of the engraftment rate, so its results are reported descriptively and treated as provisional, and the confirmatory H3 test is deferred to the full study at adequate power; H3 is not judged falsified on pilot power alone. A directional decision rule is nevertheless pre-registered: if the median chimerism of the selected arm is below that of the unselected arm and the

95% confidence-interval upper bound excludes the pre-specified “selected no worse than unselected” margin (difference ≥ −10 percentage points), then H3/H4 are paused, the programme does not enter the full-study engraftment, and it re-baselines to Track T1.

H4 (Replacement) [P]: Engraftment of low-entropy (selected or induced) autologous HSCs measurably replaces aged haematopoiesis — improved reconstitution, reduced aged-lineage skew, and restored self-renewal relative to unselected control. *Falsified if* engraftment does not improve functional readouts relative to control.

H4b (Induction) [P] (confirmatory — the production route): A low-entropy (young) state can be induced in autologous cells: an entropy-lowering protocol (controlled partial reprogramming or an entropy-reduction regimen) measurably reduces age-associated single-cell entropy below the in-vivo baseline without compromising the safety gate. The sole success endpoint is age-associated entropy; signalling-entropy (potency) changes are reported separately and are not a success or failure criterion, because partial reprogramming is expected to raise potency-associated entropy even as it lowers age-associated entropy. *Falsified if* no induced reduction in age-associated entropy is observed, or if the reduction is accompanied by a safety-gate failure. Because induction is the production route (the low-entropy fraction in an aged donor may be vanishingly small), H4b is graded confirmatory, not exploratory. Confirmatory status here reflects that induction is the make-or-break production step for the programme — if the induction protocol cannot lower age-associated entropy, the programme cannot deliver its product — not an assumption that partial reprogramming works; the endpoint is age-associated entropy only, and the null outcome (no induced reduction) is a falsification.

H4c (Partitioning-mimic) [P]: The natural mechanism of entropy partitioning (epigenetic reset at fertilisation plus asymmetric cell division) can be reproduced in vitro to produce low-entropy daughter cells from autologous cells. *Falsified if* no reproducible low-entropy progeny is produced, or if the progeny cannot be separated and selected.

H4d (Reverse-engineered meiotic partition; Track R) [P]: The reproductive entropy partition can be reproduced from autologous somatic cells: induced meiosis → haploid gametes (one active X per gamete in females) → blocked meiotic recombination (isogenicity, no genetic mismatch, no rejection) → fusion of two gametes to restore diploidy → totipotency → directed differentiation into a safe adult HSC. *Falsified if* a diploid, isogenic, functional HSC cannot be produced from somatic cells via induced meiosis, or if the safety gate fails.

H4e (Centriole-directed differentiation) [P]: A transplanted centriole, when delivered into an induced totipotent cell, is sufficient to bias differentiation toward a specific haematopoietic fate without exogenous transcription factors. *Falsified if* centriole transplantation alone does not direct lineage choice beyond the stochastic baseline,

where “beyond stochastic drift” is made operational as a lineage-bias effect size greater than two times the 95% confidence interval of the stochastic baseline estimated from at least 100 control (sham) divisions; or if the lineage outcome is not a functional adult HSC. (The primary, literature-validated route to HSC differentiation — defined transcription factors — is specified in Section 6.9 as node N5 and does not depend on H4e.)

H4f (Centriole-elimination; Track C) [P]: A safe adult HSC can be obtained by safely eliminating the centriole from an autologous somatic cell while preserving diploidy (no haploid intermediate, no meiosis, no fusion), then inducing totipotency (shared node N-TOT) and differentiating directly, without an embryo. *Falsified if* a functional, safe adult HSC cannot be produced from the acentriolar diploid state, or if the safety gate fails.

H4g (In-situ niche rejuvenation; Track T1) [P]: Resident aged autologous HSCs can be functionally rejuvenated in situ (without harvest, haploid transition, or embryo) by senolytic clearance of senescent niche cells and restoration of niche signals/systemic factors. *Falsified if* in-situ niche rejuvenation does not measurably improve HSC function, self-renewal, or the aged phenotype.

H5 (Safety) [P]: The selection/induction/return procedures do not increase genomic instability, aneuploidy, or tumorigenesis beyond predefined acceptance criteria. *Falsified if* the genome-integrity/tumorigenicity gate fails.

H6 (Automation) — engineering acceptance criterion, not a biological hypothesis. The production and quality control of young autologous cells can be automated by an AI-driven microscopy and single-cell-entropy platform with fidelity equal to or better than manual operation. Fidelity thresholds are quantified a priori: the automated entropy score must agree with the reference computational pipeline with intra-class correlation ≥ 0.90 on the same single cells; automated viability, mitotic-integrity, and ploidy calls must reproduce manual scoring with sensitivity and specificity ≥ 0.95; and the automated release decision must reproduce the manual release decision in ≥ 98% of cell products. These thresholds are pre-specified from published inter-rater reproducibility standards in image-based single-cell quality control and re-validated on pilot data before use; the 95% confidence interval of each estimate must lie entirely above the threshold to pass. The “manual” comparator is the measured inter-rater reliability of two trained technicians scoring the same images; automation must meet or exceed that measured manual level, and the manual level is reported rather than assumed. Technically, ARGUS comprises automated bright-field/fluorescence microscopy with image-based quality control (cell count, viability, mitotic-integrity, ploidy proxies) and an interface to the N8 computational entropy pipeline; its algorithms are trained on the pilot data (Section 5.7) and validated against the measured two-technician inter-rater reliability. It is an engineering and quality-control component of the registered protocol, not a

biological claim, is excluded from the falsifiable-hypothesis count and from multiple-comparison control, and is reported in the data-management and quality-control sections of the Stage 2 manuscript. The acceptance criterion is not met if any threshold fails or if automation increases the error rate of any safety/quality readout beyond acceptance criteria.

Table 6. Hypothesis–endpoint mapping and falsification thresholds.

Hypothesis	Primary endpoint	Falsification threshold	Gate / track
H1 (coupling)	entropy regressed on division history/rate	no significant association after control for cell cycle and donor age	Gate 1 / A
H2 (selectability)	selected vs. donor-matched in-vivo entropy	selected fraction not significantly lower-entropy	Gate 1 / A
H3 (no rejection)	multilineage chimerism ≥ 1% per major lineage at 16 weeks	chimerism below threshold, or immunosuppression required, or immune response	Obj 3 / A (pilot: descriptive only; confirmatory deferred to full study)
H4 (replacement)	reconstitution, lineage balance, self-renewal (serial transplant)	no improvement relative to unselected control	Obj 3 / A
H4b (induction)	induced entropy reduction vs. baseline	no reduction, or reduction with safety-gate failure	Gate 2 / A(2b)
H4c (partition-mimic)	reproducible low-entropy progeny	no progeny produced, or not separable/selectable	Gate 2 / A(2c)
H4d (meiotic partition)	diploid, isogenic, functional HSC from induced meiosis	none produced, or safety-gate failure	Track R
H4e (centriole-directed)	lineage bias of a transplanted centriole in a totipotent cell	centriole transplant alone does not direct lineage beyond stochastic drift	N5 (exploratory)
H4f	functional HSC from	none produced, or safety-	Track C

Hypothesis	Primary endpoint	Falsification threshold	Gate / track
(centriole elimination)	acentriolar diploid state	gate failure	
H4g (in-situ niche)	resident HSC function / aged phenotype after intervention	no measurable improvement	Track T1
H5 (safety)	genome-integrity and tumorigenicity gates	any gate failure	all tracks
H6 (automation)	automated vs. manual fidelity on entropy, QC, release	any pre-specified threshold not met	ARGUS

The primary outcome is functional young haematopoiesis from autologous cells; whole-body rejuvenation is out of scope.

2.1 What would falsify this programme (minimum dataset)

The programme is falsifiable as a whole at a defined point. The minimum dataset that decides the central claim comprises: (i) the coupling map (Objective 1, n ≥ 40 donors per age group); (ii) proof that the selected fraction is lower in age-associated entropy than donor-matched in-vivo HSCs (H2); (iii) a functional engraftment result against the unselected control (H3/H4); and (iv) a safety-gate result for the same product (H5). A null result on (i) — no division-rate–entropy coupling — is itself a publishable finding that directly challenges the entropy-division coupling hypothesis in HSCs and is reported as such rather than concealed; a null result on (ii)–(iv) falsifies the corresponding hypothesis and re-baselines the programme to Track T1. The full executable protocol for items (i)–(ii) is given in Section 5.7. The detailed version of this statement is in Section 13.9.

Registered scope of this Stage 1. The Stage 1 registration covers the primary arm (Track A core: H1–H4, H4b, H4c) and the parallel low-risk arm (Track T1: H4g), whose endpoints and analysis plan are specified in Sections 5, 8, and 12 and operationalised in Section 5.7. The deep tracks (Track R: H4d/H4e; Track C: H4f) and automation (H6) are presented as exploratory, gated feasibility directions outside the registered dataset: they carry no committed timeline, are reported separately as their gates are passed, and their failure does not falsify the registered hypotheses. This separation is deliberate — a Stage 1 protocol registers what it can commit to execute, and this protocol commits to Track A and Track T1.

3. The multi-track architecture and its shared nodes

3.1 Overview

The programme is organised as a primary experimental core and two exploratory directions that share a set of technical nodes. Figure 1 shows the overall architecture; Table 1 lists each track with its core nodes. Track A and Track T1 are the primary, immediately executable arms; Track C and Track R are exploratory directions entered only through the feasibility gates defined in Sections 7 and 6, and Track R is conditional on Track C confirming a permissive state.

Track A (measure–select–induce). Quantify single-cell entropy across division history and donor age; test the division-rate–entropy coupling (H1); derive youth markers; select the lowest-entropy autologous fraction (H2); where selection is insufficient, induce a low-entropy state (H4b) and reproduce the natural partitioning mechanism (H4c); return cells to the niche (H3, H4).

Track R (meiotic entropy partition; conditional, long-horizon). Reproduce the reproductive entropy partition from autologous somatic cells via germline induction, induced meiosis without recombination, haploid stabilisation, gamete fusion, zygotic genome activation, totipotency, and directed differentiation (H4d, H4e). Track R is explicitly a speculative, long-horizon direction: it is entered only if Track C confirms that the acentriolar state is permissive and only if achiasmate meiosis is made viable and euploid in a model organism first (Sections 6.3–6.4). It is not a parallel arm of equal status with Track A.

Track C (centriole elimination). Safely eliminate the centriole while preserving diploidy, induce totipotency (shared N-TOT), and differentiate directly without an embryo (H4f).

Track T1 (in-situ niche). Rejuvenate resident HSCs in the niche by senolytic clearance and niche-signal restoration (H4g), as a lower-risk parallel arm.

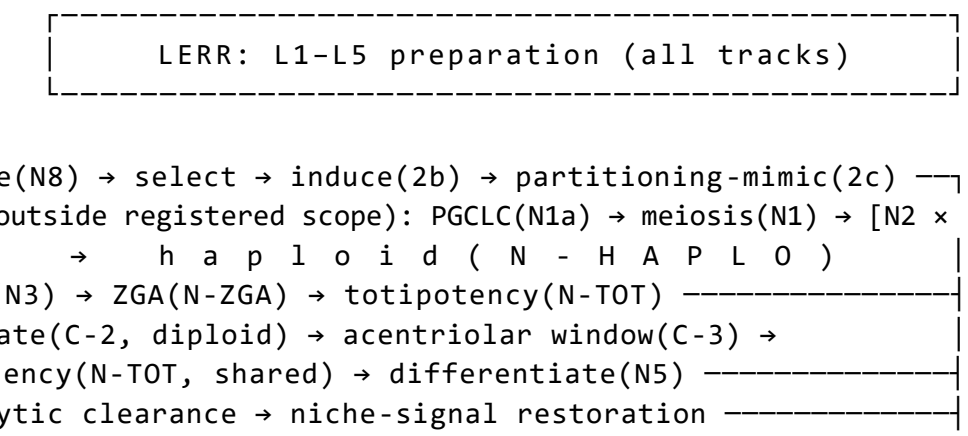
LERR (cross-cutting preparation). A staged, reversible preparation layer (ladders L1–L5) applied before the induction and partition tracks, and in reduced form before selection.

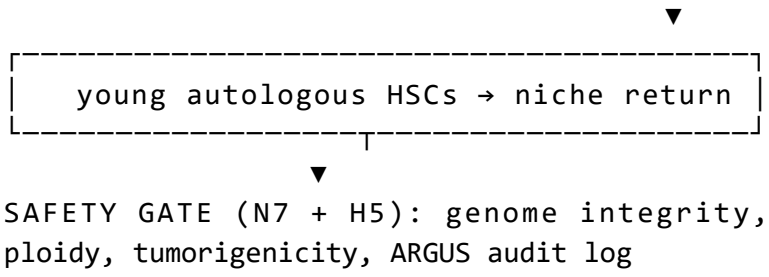
Table 1. Tracks and their core nodes.

Track	Purpose	Core nodes
A	Measure, select, induce, return	N8 single-cell entropy · youth-marker selection · induction (A1 OSK / A2 chemistry / A3 niche-mimic / A6 partitioning-

Track	Purpose	Core nodes
		mimic) · niche return · safety gate
R	Reverse-engineered meiotic entropy partition	N1a PGCLC · N1 meiosis · N2 recombination block · N-MCHK checkpoint · N3 gamete fusion · N-HAPLO haploid stabilisation · N6 imprinting control · N-ZGA/N-TOT totipotency · N5 differentiation · N4 de-novo centriole · N7 integrity · N8 verify · niche return
C	Centriole elimination, diploidy preserved	C-1 stratify · C-2 eliminate · C-3 acentriolar window · N-TOT totipotency · C-5 differentiate · C-6 rebuild · C-7 return · N7 · N8
T1	In-situ niche rejuvenation	senolytic clearance · niche-signal restoration · HSC function/entropy measurement · safety
LERR	Cross-cutting preparation	Ladder L1–L5 · Eliminate/Reprogram/Rebuild

Figure 1. Architecture of the programme. Track A and Track T1 are the primary, immediately executable arms; Track C and Track R are exploratory directions entered through the gates of Sections 6–7, with Track R conditional on Track C feasibility and on model-organism achiasmate meiosis. Shared nodes (N-TOT, N8, N5, N4, N7, niche) are implemented once and serve several tracks; the safety gate (H5) is the common exit filter; ARGUS provides the audit log across all tracks. (Rendered as a diagram in the journal version; schematic flow shown below.)





3.2 The tracks are not additive: shared nodes

The track portfolio overlaps heavily at the level of procedures. Six operations are identical across tracks and are implemented once each, with one responsible node per operation (Table 2): totipotency induction (N-TOT, shared by R and C), single-cell entropy measurement/verification (N8, shared by A, R, C, T1), differentiation-inductor delivery (N5, shared by the R-branch and C-5), de-novo centriole biogenesis (N4, shared by C-6 and R), genome-integrity/ploidy gating (N7, shared by all), and niche engraftment (shared by A, R, C, T1). This consolidation means shared methodological expertise and shared output-validation criteria: a single expert group owns the measurement standard for a node across tracks, and the acceptance criteria are the same wherever the node is used. It does not claim that the protocol or feasibility is identical in every track — the input state differs between Track R and Track C (for example, at N-TOT and N5), so the instantiation is tailored to the track while the measurement standard and validation are shared. Table 2 lists the shared procedures and their single implementations.

Table 2. Identical procedures shared across tracks, and their single implementation.

Shared procedure	Tracks	Single implementation
N-TOT totipotency induction	R ∩ C (distinct input states; protocol tailored)	one expert group (ZGA / induced totipotency); protocol adapted to input state
N8 single-cell entropy (measure / verify)	A ∩ R ∩ C ∩ T1	one bioinformatics lead
N5 differentiation-inductor delivery	R-branch ∩ C-5	one differentiation-mechanism node
N4 de-novo centriole biogenesis / rebuild	C-6 ∩ R	one centriole-biogenesis group

Shared procedure	Tracks	Single implementation
N7 genome-integrity / ploidy gate	A ∩ R ∩ C ∩ T1	one safety-genomics node
Niche engraftment	A ∩ R ∩ C ∩ T1	one niche-biology node

3.3 Acentricity, ploidy, and the logic of the two deep tracks

Track R and Track C differ in one decisive respect. Track R passes through a haploid intermediate (gametes) to reach totipotency, and thereby solves, en route, the female two-X dosage problem: a haploid cell carries one active X, so the X-inactivation mosaic inherent to diploid female somatic cells is bypassed at the haploid stage. Track C avoids the haploid state entirely (the cell remains diploid throughout) and instead uses the acentriolar window as the reprogramming-primed state. Both tracks require a robust totipotency-induction node (N-TOT) and both converge on direct, embryo-free differentiation (N5). The two tracks are therefore complementary in risk: Track R is the deepest partition but the most fragile (haploid intermediates, checkpoint biology); Track C is lighter but depends on the acentriolar window being a permissive state for totipotency induction, a proposition that is empirically testable (Section 7).

4. LERR: the cross-cutting preparation layer

LERR is the shared preparation strategy applied before the induction and partition tracks (2b–2e) and in reduced form before pure selection. Its purpose is to stage and condition autologous cells so that any subsequent manipulation acts on cells that are ready, observable, and revertible.

4.1 Ladder L1–L5

L1 — Stratification. Autologous cells are stratified by post-translational modification (PTM) load on the tubulin code, by centriole age (mother vs. daughter centriole), and by baseline single-cell entropy. The purpose is to select the best-responding donor cell and to establish the pre-manipulation baseline against which every later measurement is compared.

L2 — Reversible PTM modulation. The tubulin code is modulated reversibly with inhibitors of tubulin-modifying enzymes (HDAC6, CCP5/CCP6, TTLL families). The defining constraint is reversibility: every intervention has a rollback trigger, the activation of p53, which aborts the procedure and returns the cell to a baseline state. This gives the ladder its safety property at the earliest stage.

L3 — Half-elimination of the mother centriole. The aged mother centriole is removed while the daughter centriole is retained as a template. The operational justification is the

generic partitioning-mimic rationale — purging aged structures, as gametogenesis does (Goodman et al., 2020) — and the operational method is experimental: reversible centriole depletion by PLK4 inhibition as established with centrinone (Wong et al., 2015), with de-novo reassembly documented after loss (La Terra et al., 2005; Uetake et al., 2007). No step relies on the centriole-division-counter hypothesis, which this programme does not adopt (Section 1.5).

L4 — Acentriolar priming. Cells are primed with low-dose DUX4 — the conserved activator of cleavage-stage genes and MERVL/HERVL retroelements (Hendrickson et al., 2017) — in combination with a p53/p38 block (pifithrin-α and SB203580). The rationale is twofold: DUX4 is an established activator of the totipotent/zygotic program, and the p53/p38 block prevents the checkpoint-mediated apoptosis that otherwise follows loss of the centrosome (see Section 7.2). This creates the acentriolar, reprogramming-primed window. The p53/p38 blockade targets the documented barriers to acentriolar survival — p53-dependent apoptosis after prolonged prometaphase (Bazzi & Anderson, 2014) and a p38-dependent G1 arrest (Uetake et al., 2007).

L5 — Readiness gate. Entry to the next stage is permitted only if: viability ≥ 90%, mitosis is normal (no mitotic catastrophe), p53 is not activated, genome integrity is confirmed (low-pass WGS), and the entire process is logged by the automated platform (ARGUS). The gate is absolute: any failure aborts the ladder.

4.2 Eliminate–Reprogram–Rebuild

Where a track requires centriole manipulation, the ladder is followed by the three canonical operations. **Eliminate:** removal of the aged centriole, residual epigenetic marks, and (where relevant) telomere-associated stress. **Reprogram:** in the acentriolar window, activation of the reprogramming program (DUX4, KDM4D, DPPA3). **Rebuild:** de-novo biogenesis of young centrioles along the canonical pathway PLK4 → SAS-6 → STIL → CPAP (Section 7.6).

4.3 Reduced form

Where a track does not require centriole manipulation (pure selection, Track A core; Track T1), LERR is applied in reduced form: L1 (stratification) and L5 (readiness gate) only.

5. Track A: measure, select, induce, return

5.1 Objective 1 — the coupling experiment (Years 1–2)

Procedure. Autologous CD34+ HSCs are isolated from peripheral blood or bone-marrow aspirates of healthy donors stratified into young, middle-aged, and old groups (≥ 20 per group). Division history is tracked ex vivo by CFSE/PKH26 dilution and by clonal

lineage analysis, with time-resolved sampling (24, 48, 72, 96 h) so that the effective division rate (the log-slope of dye-peak proportions over time) is estimated separately from cumulative division number; parallel single-cell RNA-seq and scATAC-seq are collected from the same cells. HSCs demonstrably count and remember their self-renewal divisions (Bernitz et al., 2016), and divisional history measurably shapes HSC function during homeostasis (Qiu et al., 2014), so a division-linked accumulation of transcriptomic entropy is mechanistically plausible; whether it exists, and at what magnitude, is the hypothesis H1. H1 is stated as an association (division history and entropy are positively associated) rather than a causal claim: the pilot estimates the association and its strength, and causality is a full-study design question addressed by a division-induction arm (inducing division in otherwise quiescent HSCs and testing whether entropy rises), which is planned but not assumed. Candidate mechanisms by which division history could accumulate transcriptomic entropy are named as hypotheses rather than claims: accumulation of replicative stress and DNA damage per division, asymmetric inheritance of aged histone marks and DNA strands between daughters, cell-cycle-coupled transcriptional noise, and age-associated cryptic transcription (aberrant transcription-start-site usage in aged cells) Each is testable in the Objective 1 atlas and is operationalised concretely — for example, a replicative-stress module score (CDKN1A, TP53, GADD45A and p53-target genes) computed per division peak — and none depends on a single molecular model, including the centriole-counter model. Age-associated single-cell entropy is computed per cell as its deviation from a well-ordered type-specific transcriptomic reference, cross-checked with a single-cell ageing clock (Buckley et al., 2023) and with a manifold-deviation entropy measure (Yang et al., 2026); signalling (potency) entropy (Teschendorff & Enver, 2017) is computed only as a secondary, potency-flagged analysis, never used as the selection criterion. Entropy is regressed on division number/rate, controlling for donor age and cell-cycle state.

Interpretation and branching. If a significant division-rate–entropy association is found (H1), the induction protocols of Objective 2b are designed to target its causes. Cell-cycle state is included as a covariate in every model, and the association is reported both cell-cycle-adjusted and unadjusted; a G0/G1-restricted sensitivity analysis is reported alongside, but it is not the primary analysis, because division tracking by dye dilution requires dividing cells and a G0/G1 restriction would systematically exclude the cells whose division history is the variable of interest. The primary statistical model uses the full random structure — a random intercept for donor, a random slope for division within donor, and a nested term for donor-by-division-peak to account for the non-independence of cells sharing a donor and a division peak. A division-independent validation arm (label-retention or inducible-division tracking) is planned at full study to disentangle “has divided many times” from “is currently cycling fast”; until then H1 is reported as an association. The deliverable is a quantitative map of the coupling (its

existence, sign, and magnitude) which is the empirical foundation of the whole selection logic.

5.2 Objective 2 — youth markers and the selection pipeline (Years 2–3)

Procedure. From the Objective 1 atlas, a youth signature is defined as the set of transcriptomic/regulatory programs that are differentially low-entropy in the youngest functional fraction. A selection pipeline is then built: FACS sorting of the lowest-entropy HSC fraction on the basis of signature surface markers, with single-cell RNA validation of the sorted product. Two verification requirements are fixed in advance: the selected cells must be measurably lower in entropy than donor-matched in-vivo HSCs (H2), and the signature must be stable in culture.

Fallback. If no stable surface signature emerges, single-cell entropy scoring is applied directly to freshly drawn cells with index-sorted single-cell validation, rather than relying on surface markers alone. Two distinct operations must not be conflated: division tracking sorts cells by dye-dilution peak into lysis buffer (Section 5.7.3, item iii), which is a tracking operation, not an entropy selection; entropy selection itself is either (a) surface-marker FACS, where the markers are an atlas-derived approximation of the low-entropy state, or (b) retrospective index-sorted validation — cells are sequenced, their age-associated entropy is computed, and the lowest-decile fraction is identified by index. Because post-hoc index sorting cannot return a usable live-cell product (cells are lysed for sequencing), (b) serves to validate the proxy (a) and to discover surface markers for the next proxy round; prospective selection of the transplant product always operates on live cells via (a).

5.3 Objective 2b — induction of youth (Years 2–3)

Selection alone is expected to be insufficient in aged donors, where the low-entropy fraction may be vanishingly small. Objective 2b therefore develops induction as a *production* route: a low-entropy state is made, not harvested. Two families of intervention are tested on LERR-gated autologous HSCs. (i) Brief, pulsed partial reprogramming by the Oct4–Sox2–Klf4 (OSK) factor set, first shown to induce pluripotency in somatic cells (Takahashi & Yamanaka, 2006), delivered as modified mRNA (Warren et al., 2010) and applied in the short, non-converting pulses established to improve markers of ageing in vivo (Ocampo et al., 2016; Lu et al., 2020; Sahu et al., 2024), titrated to reduce entropy without full iPSC conversion. Pulses are administered as short modified-mRNA transfections (transient OSK exposure of one to three days followed by a recovery period, per the published protocol of Warren et al., 2010) with dose and pulse number titrated per donor and single-cell entropy and safety readouts taken at every passage. (ii) Entropy-reduction culture conditions, including metabolic and niche-mimetic regimens. Single-cell entropy is measured before and after each intervention; the reduced-entropy state must be stable and revertible, and the safety

gate must remain intact (H4b, H5). If a significant division–entropy coupling was found in Objective 1, the induction protocol is targeted at the identified causes rather than applied generically. One caveat is explicit: partial reprogramming may raise potency-associated entropy even while reducing age-associated entropy, and published single-cell analyses show that reprogramming does not uniformly lower entropy (Yang et al., 2026). The induction endpoint is therefore defined as a reduction in *age-associated* entropy with the safety gate intact; potency-entropy changes are reported separately rather than treated as the outcome.

5.4 Objective 2c — partitioning-mimic (Years 2–4)

Nature produces a young cell not by rejuvenating an old one but by partitioning entropy: it builds a fresh, low-entropy compartment (the offspring) apart from the aged soma, through epigenetic reset at fertilisation, asymmetric cell division, and germline quality control. Objective 2c reproduces each of these mechanisms in vitro and measures the entropy of the progeny. Three sub-routes are specified.

(i) Engineered asymmetric division. Cells are induced to divide so that one daughter inherits the fresh structural template (new centriole, new DNA strand) and the other the aged one, informed by the centriole-division-counter model (Tkemaladze, 2023). The low-entropy daughter is then selected by entropy scoring. If segregation is stochastic rather than deterministic, the design explicitly falls back to entropy-based single-cell selection of whichever daughter is low-entropy — the requirement is a reproducible, selectable low-entropy progeny, not a deterministic mechanism (H4c).

(ii) ZGA-like partial reprogramming. Partial reprogramming is used as an in-vitro analogue of the fertilisation epigenetic reset (the demethylation waves of zygotic genome activation), mimicking the natural epigenetic entropy partition.

(iii) Germline-style selective degradation. Gametogenesis is not merely a mitochondrial bottleneck; it is a multi-level quality-control process that purges damaged structures of all classes. The evidence base is specific and PMID-verified: gamete production eliminates age-dependent organelle and protein damage in yeast meiosis and beyond (Goodman et al., 2020); oocyte maturation triggers clearance of carbonylated proteins and aggregates through lysosomal microautophagy in the immortal germline (Samaddar et al., 2021); SPATA33 acts as a mitophagy receptor for selective mitochondrial degradation in the mammalian germline (Xu et al., 2021); selective autophagy in spermatogenesis targets damaged organelles and protein aggregates (Lv et al., 2020); ClpP maintains mitochondrial integrity and meiotic progression in spermatocytes (Feng et al., 2026); mitochondrial redox homeostasis links organellar stress surveillance to both germline and somatic integrity through the ATFS-1/UPRmt axis (Valenzuela-Villatoro et al., 2026); and mitochondrial microautophagy selectively removes damaged mitochondrial subdomains (Zhang et al., 2026). Objective

2c accordingly induces mitophagy, proteostasis clearance, and UPRmt in autologous cells to purge organellar entropy before producing the low-entropy progeny. The produced progeny must be selectable and stable (H4c).

5.5 Objective 3 — autologous niche engraftment (Years 3–4)

Procedure. The selected or induced low-entropy autologous HSCs, or totipotency-derived HSCs from the deep tracks, are transplanted into NSG-class immunodeficient mice, with engraftment assessed by human CD45+ chimerism (Hasgur et al., 2016). The experimental arm is compared with unselected autologous HSCs from the same donor. Primary endpoints at 16 weeks: multilineage engraftment, lineage balance, and self-renewal as assayed by serial transplantation. Supporting assays: peripheral-blood chimerism, lineage output, and colony-forming units. **Risk mitigation.** If the NSG model does not fully support human HSC self-renewal, the readout is complemented with in-vitro niche coculture (mesenchymal/osteoblast feeder) and a transcriptional ageing clock.

5.6 Track A summary

Track A is the only track that is implementable in the first two years at moderate risk, because every operation in it is already individually published: single-cell entropy computation, division tracking, FACS selection, pulsed partial reprogramming, and autologous engraftment in humanised mice. Its novelty lies entirely in their integration around entropy as the selectable and inducible endpoint. Section 5.7 specifies the first experiment in full, executable detail.

5.7 Pilot protocol: the immediately executable minimum dataset

This subsection specifies the first experiment of the programme. It is designed to be executable within 12–18 months, to produce the minimum dataset of Section 2.1 (items i–ii), and to be written so that another laboratory can replicate it. It is a pilot: sized for effect estimation and variance, not for a definitive test, with a pre-registered rule that a null result is reported as a publishable negative finding. The full step-by-step operational detail for this pilot — materials, doses, FACS gates, computational pipeline parameters, and acceptance thresholds — is provided in the companion methods document, *Protocol: division tracking, index sorting, and single-cell entropy in human HSCs* (Tqemaladze, 2026). Section 5.7 is self-contained: all decision-relevant parameters and analysis rules needed to evaluate the pilot are present in this subsection (the entropy-computation parameters themselves are in Section 10 of this article), and the companion Protocol is optional operational depth for wet-lab execution, not a document that reviewers must consult to assess the design. The distinction between the two layers is explicit: decision-relevant parameters (those that affect whether the hypotheses are testable and how results would be interpreted) are in the article body;

technical-execution parameters (reagent catalogue numbers, instrument settings, computational-environment configuration) are the companion/supplementary layer.

5.7.1 Objective and decision logic. Primary objective (H1): estimate the association between division history/rate and age-associated single-cell entropy in human HSCs, controlling for cell-cycle state and donor age. Secondary objective (H2, pre-pilot): test whether a low-age-associated-entropy HSC fraction can be isolated by index-sorted selection and whether it is measurably lower in age-associated entropy than donor-matched in-vivo HSCs. Decision rule: a significant association scales the study to the full design (n ≥ 40 per age group) and targets induction at its causes; a null association is written up as a negative result that challenges the entropy-division coupling hypothesis; non-concordant entropy measures are reported as a methods finding and the more function-correlated measure is used.

5.7.2 Design overview.

Element	Specification
Study type	Cross-sectional, multi-donor, single-cell atlas + index-sorted validation
Donors	n = 12 (≥ 10 analyzable; recruit 15): 4 young (< 30 y), 4 middle (30–60 y), 4 old (> 60 y)
Source	Peripheral blood (G-CSF mobilised) or bone-marrow aspirate; autologous, consented
Cell type	CD34+ HSCs (Lin−CD34+CD38−CD45RA−CD90+) with a CD34+CD38+ progenitor gate
Division tracking	CFSE/PKH26 dilution ex vivo + dye-peak index sorting (0, 1, 2, ≥ 3 divisions)
Single-cell assays	scRNA-seq (10x 3′ v3); scATAC-seq optional for regulatory-level cross-validation
Entropy metrics	age-associated entropy; primary selection via whichever candidate passes validation (re-derived HSC clock — peer-reviewed framework, re-derivation required; manifold-deviation — preprint, exploratory until validated); VarID2 noise cross-check; signalling entropy potency-flagged secondary
Primary contrast	age-associated entropy vs. division number/rate, mixed-effects model (donor random effect)

Element	Specification
Timeline	12–18 months

Power: the pilot (n = 12) is intentionally below the n ≈ 23 (paired, 90% power) of Section 12; it is sized to detect a donor-level correlation of r ≈ 0.5–0.6 and to estimate variance for the full design.

5.7.3 Procedures. Operational detail shared with the companion Protocol (Tqemaladze, 2026, *Protocol: division tracking, index sorting, and single-cell entropy in human HSCs*) is referenced rather than duplicated; the decision-relevant parameters are recorded here. (i) Ethics approval and protocol registration (OSF) precede recruitment; inclusion criteria exclude active malignancy, recent transplantation, and known clonal haematopoiesis, which is screened by low-pass WGS on the same sample; donors with a clonal-haematopoiesis variant allele fraction above 2% in driver genes are excluded from the primary analysis or analysed as a covariate. (ii) Mononuclear cells are isolated by density gradient; CD34+ enrichment to ≥ 90%; FACS gates for LT-HSC and progenitors; viability ≥ 95%. (iii) Freshly isolated HSCs are labelled with CFSE (0.5–1.0 μM) or PKH26 and cultured at limiting dilution in serum-free medium with SCF/TPO/FLT3L for 72–96 h; at harvest, cells are sorted by dye-dilution peak directly into lysis buffer; a fresh, un-cultured aliquot is the in-vivo division-zero reference, a no-cytokine control distinguishes driven from artefactual division, and a dye-only control (labelled cells without a proliferation stimulus, entropy compared against unlabelled cells of the same donor) isolates the metabolic effect of the label itself from the effect of division; the dye-only comparison is a formal equivalence test with a pre-specified margin (two one-sided tests, margin $|\Delta\text{entropy}| \leq 0.2$ SD units, set at the conventional small-effect benchmark; Cohen, 1988), not a mere “not significantly different” claim, and the known amine-binding and mitochondrial-perturbation effects of CFSE are acknowledged as the reason this control is mandatory. Division number is computed from dye dilution as $\text{division_number} = \log_2(\text{MFI_undivided} / \text{MFI_peak})$, where MFI_undivided is the geometric-mean fluorescence of the division-zero reference and MFI_peak is the geometric-mean fluorescence of the sorted peak; peaks are assigned to integer division numbers by a fixed gating protocol (FlowJo proliferation modelling or a fixed manual gate set, recorded before analysis), and the ≤ 10% peak-overlap acceptance criterion is computed from the fitted peak distributions. The effective division rate is computed as $\text{rate} = \Delta(\text{mean division number})/\Delta t$, using at least three time points (24, 48, 72 h) per donor, and is reported as a separate estimand from cumulative division number. (iv) scRNA-seq at ≥ 5,000 cells/donor/peak and ≥ 20,000 reads/cell; scATAC-seq at ≥ 2,000 cells/donor where budget allows. (v) Entropy is computed by the fixed pipeline of Section 10 (QC, normalisation, batch integration, cell-cycle scoring, annotation), with the primary HSC re-derived clock component and the four-step manifold-deviation procedure as exploratory; concordance of $\rho \geq 0.6$ between the clock

and manifold scores is required before either is used as a selection readout. (vi) The primary statistical model is a linear mixed-effects model (age-associated entropy ~ division number + cell-cycle state + donor age). The registered primary specification is the full structure — a random intercept for donor, a random slope for division within donor, and a nested donor-by-division-peak term — and this specification is identical across the pilot and the full study; only the sample size is re-estimated. In the pilot (n = 12), the nested variance component may be non-estimable, in which case reduced models (intercept-only, intercept + slope) are reported as feasibility estimates and do not change the registered specification. H2 uses a paired Wilcoxon on index-sorted lowest-decile vs. in-vivo HSCs; multiple testing by Benjamini–Hochberg FDR q = 0.05 within the confirmatory family (H1–H4) and the exploratory family (H4b–H4g) separately, with Bonferroni sensitivity. (vii) A pre-registered secondary analysis quantifies the contribution of culture itself to the entropy signal: the entropy of index-sorted division-peak-0 cells is compared against the fresh, un-cultured LT-HSC reference of the same donor; this comparison is a formal secondary analysis, not only a control.

5.7.4 Milestones and timeline.

Month	Milestone	Deliverable
0–2	Ethics, consent, protocol registration, assay optimisation	Registered protocol
2–4	Donor recruitment (n = 12), sample collection	Banked samples, QC report
4–6	HSC enrichment + division tracking	Division-peak suspensions
5–8	scRNA-seq (+ scATAC) libraries	Raw data (FASTQ) deposited
8–12	Computational pipeline: QC, integration, entropy, concordance	Atlas + metric QC
12–14	Primary analysis (H1), H2 pre-pilot, sensitivity	Analysis scripts + figures
14–16	Manuscript (positive or null), GEO + code deposit, preprint	Manuscript v1
16–18	Review; scale-up decision or re-baseline to Track T1	Decision memo

5.7.5 Budget (indicative). Personnel (0.5 FTE × 18 mo) €45K; scRNA-seq (12 donors × peaks) €60K; scATAC-seq (optional) €30K; HSC enrichment/FACS/division tracking €18K; recruitment €12K; ethics/coordination €5K; QC/compute €8K; open access €5K; total ≈ €183K with scATAC.

5.7.6 Risks and mitigations. Donor attrition / low CD34+ yield (recruit 15, marrow backup); ex-vivo division altering entropy (fresh in-vivo reference, no-cytokine control, cell-cycle-adjusted primary analysis); non-concordant entropy metrics (pre-registered rule: use the more function-correlated measure); cell-cycle confounding (cell-cycle state as covariate, adjusted and unadjusted); clonal haematopoiesis in older donors (screening, exclusion or covariate); null result (planned as a publishable negative).

5.7.7 Deliverables. (i) Public single-cell atlas of division-tagged human HSCs across age (GEO); (ii) pre-registered analysis code and protocol (OSF/GitHub); (iii) a manuscript, *Division history and age-associated transcriptional entropy in human haematopoietic stem cells*, publishable whether the coupling is present or absent; (iv) a decision memo on scaling to the full study or re-baselining to Track T1.

6. Track R (exploratory, outside registered scope): reverse-engineering the reproductive entropy partition

Track R is the deepest induction route and the highest risk. It reproduces, from an autologous somatic cell, the chain of events by which nature produces a young diploid cell: germline induction, meiosis, haploid gametes, fusion, and the epigenetic reset of the resulting zygote. Each node is described below with its rationale, evidence, procedure, and failure condition.

6.1 Node N1a — somatic-to-PGC-like induction

Rationale. Meiosis in mammals is not induced directly in a somatic cell; it is entered from a germline state. In-vitro gametogenesis (IVG) proceeds from pluripotent stem cells through primordial-germ-cell-like cells (PGCLCs) to gametes, in both mouse and human systems. A somatic cell must therefore first be driven to a PGC-like state before meiotic competence is established.

Procedure. Autologous somatic cells are reprogrammed to a pluripotent or germline-competent state, then specified to PGCLCs by the canonical cytokine combination (BMP4, WNT3A, SCF) with the transcription factors BLIMP1, PRDM14, and AP2γ, following the IVG lineage. The route has been completed end-to-end in the mouse, where oocytes derived from in-vitro PGCLCs produced fertile offspring (Hayashi et al., 2012); the specification of human germline fate through SOX-family factors is an established, actively extended area (Pierson et al., 2019).

Failure condition. No PGCLC specification, or PGCLCs that cannot be maintained and expanded to sufficient numbers. An acknowledged limitation is that human PGCLCs in culture readily de-differentiate and that their differentiation to oocytes remains incomplete; the PGCLC node of Track R is therefore validated in the mouse first, with human application as the long-horizon step.

6.2 Node N1 — induced meiosis

Rationale and evidence. Meiotic entry in mammals is governed by STRA8 and MEIOSIN; STRA8 marks the decision to enter meiosis in germ cells (Baltus et al., 2006), and MEIOSIN directs the switch from mitosis to meiosis (Ishiguro et al., 2020). DAZL and BOULE regulate later germline development. These factors constitute a defined molecular entry point.

Procedure. The PGCLC-like cells are induced to enter meiosis by activation of STRA8/MEIOSIN/DAZL/BOULE, with staged culture into the meiotic prophase programme.

Failure condition. No meiotic entry, or entry with grossly abnormal chromosome dynamics.

6.3 Node N2 — blockade of meiotic recombination for isogenicity

Rationale. Both gamete-like cells in this design derive from one donor genome. Meiotic crossing over generates new allele combinations, so without intervention the two gametes would be genetically recombinant and their fusion would create a genetic mismatch — the source of immunogenic neo-antigens and, ultimately, rejection. Blocking crossing over preserves isogenicity: the fused product is identical to the donor genome and is therefore immunologically self. This node implements the isogenicity that makes the returned product immunologically self, which is the basis of the conditional no-immunosuppression claim of Section 11.

Procedure. Meiotic recombination is initiated by SPO11-generated double-strand breaks (DSBs) and executed through DMC1/RAD51 strand invasion. Three intervention points are specified: ablation of SPO11 (no DSBs, maximal isogenicity), inhibition of DMC1/RAD51 (blocked strand invasion), and titration of DSB number (partial suppression). Isogenicity is verified by whole-genome sequencing and SNP profiling before any fusion or transplantation.

Failure condition and its resolution (hard gate). Full recombination blockade confronts two fundamental biological barriers, and the design treats them as such rather than as manageable obstacles. First, chiasmata hold homologous chromosomes together for segregation in meiosis I; without them, non-disjunction and aneuploidy are the expected outcome. This is not hypothetical: in Spo11-less meiosis, viable spores

are rare and, when they arise, show chromosome-length-dependent aneuploidy (Kawashima et al., 2023). Second, the pachytene checkpoint eliminates cells with unpaired or DSB-free chromosomes through ATM signalling, so fully achiasmate meiosis arrests or dies. The design therefore proceeds by titration and checkpoint modulation (N-MCHK), but with an explicit feasibility gate: if achiasmate meiosis cannot be made viable and euploid in a model organism within the feasibility window, Track R is stopped and isogenicity is sought by alternative routes, which are themselves research objectives rather than assumptions. The three-way constraint is stated explicitly as the central open problem: full recombination block destroys segregation, retained recombination destroys isogenicity, and partial suppression leaves residual recombination with residual immunogenic divergence; no published combination of ATM modulation with partial SPO11 ablation has produced euploid achiasmate products in a mammal, and Track R is contingent on that demonstration.

Alternative isogenicity strategies (discussed, not assumed). Two routes that do not depend on full achiasmate meiosis are specified. (i) Site-specific recombination restriction: a dCas9–SPO11 fusion protein could direct double-strand breaks to defined loci, retaining enough chiasma formation for segregation while restricting crossover to non-immunogenic, non-coding regions; the isogenicity claim is then verified by whole-genome sequencing of the products rather than by the absence of recombination. This route is graded [H] (speculative engineering): a dCas9–SPO11 fusion protein is not an established reagent in the published literature, so its feasibility is part of the Track R gate rather than an assumption. (ii) Haploid parthenogenetic direct differentiation: a haploid product that never passes through fusion is differentiated directly to an HSC, avoiding the recombination problem entirely; this route must confront the imprinting and dosage issues of uniparental genomes (managed at node N6), and both routes are feasibility-gated in the same way as the main Track R design.

6.4 Node N-MCHK — management of the pachytene checkpoint

Rationale. The checkpoint that destroys achiasmate cells is the principal biological obstacle to the isogenic meiosis that N2 requires. It is ATM-dependent and operates at the pachytene stage of meiotic prophase. Independent work makes this barrier concrete in the mouse oocyte, the system in which the Track R gate is first tested: the DNA-damage checkpoint eliminates mouse oocytes with chromosome-synapsis failure through a CHK1/CHK2-to-p53/p63 pathway (Rinaldi et al., 2017), and BRCA1 activates the chromosome-asynapsis checkpoint to eliminate recombination-defective oocytes (Bai et al., 2024).

Procedure. Three strategies are pursued in combination: titration of recombination suppression (retaining synapse); modulation of ATM signalling during meiosis to weaken the checkpoint without wholesale loss of the DNA-damage response; and, in

parallel, development of alternative mechanisms for holding homologues together in the absence of chiasmata. The overall design goal is an achiasmate meiosis that survives to produce viable, correctly segregated haploid products. The constraint that determines whether the track proceeds is ploidy rather than the survival of meiosis per se: even a rescued achiasmate meiosis yields, at best, products whose euploidy is unproven, and aneuploid gametes would fuse to aneuploid zygotes — a direct violation of the N7 ploidy gate and of the goal of a safe adult HSC. Track R is therefore contingent on demonstrating euploid achiasmate products in a model organism; no mammalian system has yet achieved this, and ATM suppression sufficient to bypass the checkpoint is expected to compromise genome stability, a conflict that Section 6.3 treats as an open, gated problem rather than a solved one. The gate is operationalised so that it can be judged, not merely asserted: model organisms are mouse (first) and yeast (mechanistic); euploidy is assessed by karyotype plus low-pass whole-genome sequencing of at least 100 haploid products, requiring ≥ 80% euploid; and the gate is judged failed if these criteria are not met within a five-year window. The gate is framed as sequential monitoring rather than a fixed pass/fail snapshot: euploidy is tracked as products accumulate, with pre-specified stopping rules (the gate is judged failed if the observed euploid fraction and its confidence interval fall below the 80% threshold at a pre-registered interim), and the binomial uncertainty of the 100-product sample is acknowledged in the stopping rule. Two independent layers are distinguished: the feasibility gate (whether the products are euploid) and the safety gate (whether the products are genomically stable and non-tumorigenic, Section 11). If an operation passes the feasibility gate but persistently triggers the safety-gate alarms, Track R is terminated rather than iterated. Consistent with Section 2, Track R is a speculative feasibility study outside the registered scope, not a committed arm.

Failure condition. Apoptotic loss of meiotic cells at pachytene despite titration, with no rescue by checkpoint modulation. A further constraint is developmental: human meiosis has not been reconstituted beyond early prophase in vitro, and human PGCLC-derived oogenesis remains incomplete. Track R is therefore explicitly a long-horizon, speculative arm whose feasibility is tested in model organisms before any human claim; the manuscript does not assert that full human meiosis in vitro is currently achievable.

6.5 Node N-HAPLO — haploid stabilisation

Rationale. Two functions justify the haploid stage, and both must be engineered deliberately. First, a haploid cell carries one active X chromosome, solving the female two-X dosage problem at the haploid stage (one active X per gamete; the X-inactivation mosaic of diploid female somatic cells is bypassed). Second, haploid cells are needed for fusion. However, haploid intermediates are unstable: spontaneous diploidisation is common.

Procedure. Haploid products are stabilised by DNA-content FACS sorting, by culture conditions that suppress spontaneous diploidisation, and by p53-pathway modulation where compatible with the safety gate. Haploid mammalian stem cells are an established, viable system in both mouse and human (Sagi et al., 2016; Edwards et al., 2021).

Failure condition. Irreversible spontaneous diploidisation before fusion, or haploid products that cannot be expanded to usable numbers.

6.6 Node N3 — fusion of two gamete-like cells

Rationale. Fusion of two haploid products restores diploidy, mimicking fertilisation, and produces the totipotent (zygote-like) starting point from which directed differentiation proceeds.

Procedure. Two stabilised haploid products from the same donor are fused to restore diploidy. Ploidy is verified immediately after fusion and throughout subsequent culture.

Failure condition. No fusion, or fused products with aneuploidy that cannot be rescued.

6.7 Node N-ZGA — zygotic genome activation

Rationale. The fused genome is transcriptionally inactive until zygotic genome activation (ZGA) is triggered: minor ZGA at the zygote stage and major ZGA at the two-cell stage, driven by factors including Nr5a2, DUX4, and DPPA3. Without ZGA, totipotency and differentiation cannot be initiated.

Procedure. After fusion, the maternal-to-zygotic transition is induced by activating the ZGA program (Nr5a2/DUX4/DPPA3), reproducing the minor and major ZGA waves in the in-vitro product; DUX/DUX4-family factors are the conserved drivers of cleavage-stage gene and MERVL/HERVL activation (Hendrickson et al., 2017).

Failure condition. No ZGA, or an abortive transition with genome silencing persisting.

6.8 Node N-TOT — totipotency induction (shared)

Rationale. The meiosis–fusion product must be genuinely totipotent (capable of giving rise to a full organism) before direct differentiation can be claimed as embryo-free. Totipotency is validated by lineage and pluripotency readouts and, in the most stringent form, by full-organism development in an appropriate model.

Procedure. The totipotent program is activated from the zygote-like state (ZGA-like / DUX4/DPPA3/Nr5a2; induced-totipotency templates). This node is consolidated under one responsible expert group. The two input states differ — the meiosis–fusion product is zygote-like, while the Track C input is an acentriolar diploid cell — so the induction

protocol is tailored to the starting state; the node is shared at the level of output validation (a defined totipotency readout), not assumed to be a single protocol.

Failure condition. Failure to achieve or validate totipotency, in which case the direct-differentiation claim of both deep tracks collapses and the track is abandoned.

6.9 Node N5 — direct differentiation without an embryo (shared)

Rationale. From the totipotent cell, the goal is to obtain a cell of the desired differentiation directly — without the use of an embryo's life. This requires identifying the mechanism of differentiation.

Procedure (primary route — defined transcription factors). The totipotent cell is directed to a haematopoietic fate by defined transcription factors, the only route with published functional validation. Human pluripotent stem cells can be driven to haematopoietic stem and progenitor cells by the factors RUNX1b and ERG (Sugimura et al., 2017); committed haematopoietic cells can be reprogrammed to engraftable induced HSCs with defined factors (Riddell et al., 2014); and multipotential haematopoietic progenitors can be obtained from human pluripotent cells by respecification of lineage-restricted precursors (Doulatov et al., 2013). The primary N5 protocol applies this factor set to the induced totipotent cell and validates the product as an adult HSC by the lineage, function, and safety assays of Section 11. One caveat is stated: the RUNX1b/ERG route has published functional validation for haematopoietic stem and progenitor cells, but the long-term self-renewal and repopulation capacity of such cells has been contested in independent replication; N5 therefore re-validates self-renewal by serial transplantation (Section 11) within the Objective 1 atlas framework rather than assuming it, and, where the defined-TF route fails replication in the programme's own hands, the secondary operational fallback is directed differentiation of autologous iPSCs into HSCs by the established pluripotent-to-HSPC protocols, with the same validation gates.

Exploratory sub-hypothesis (centriole transplant, H4e). The proposal that a transplanted centriole carries a portable differentiation determinant and sets cell fate directly is not established; published evidence links centrosome inheritance to fate in asymmetric stem-cell division, not to direct differentiation from a totipotent cell. Centriole transplantation is therefore tested as an exploratory sub-hypothesis in parallel with the primary TF route, and only where the acentriolar state makes it feasible; it is not the operational basis of N5.

Failure condition. No differentiation mechanism is identifiable, or neither centriole transplantation nor the fallback drives the totipotent cell to a functional adult stem cell.

6.10 Node N4 — de-novo centriole biogenesis (shared)

Rationale. The mature adult stem cell requires centrioles; where the cell has passed through an acentriolar or zygote-like state, young centrioles are built de novo.

Procedure. De-novo biogenesis along the canonical pathway PLK4 → SAS-6 → STIL → CPAP, with validation that exactly the correct number of centrioles is produced (no supernumerary centrioles, no aneuploidy).

Failure condition. Acentriolar cells cannot produce faithful centrioles, or biogenesis is unfaithful (extra centrioles, mitotic errors).

6.11 Node N7 — genome integrity and ploidy gate (shared, all tracks)

Procedure. Throughout the track: karyotype, low-pass whole-genome sequencing, on-target/off-target integrity assessment of every manipulation, clonal-haematopoiesis surveillance, teratoma/tumorigenicity assay (10^6 cells subcutaneously, 12 weeks), and serial-transplantation safety. No rejuvenation claim is admissible unless the genome-integrity and tumorigenicity gates pass (H5). The aneuploidy risk introduced by achiasmate meiosis (N2) and by haploid intermediates (N-HAPLO) is monitored continuously, not only at endpoints. Because aneuploid gametes fuse to aneuploid zygotes, euploidy of the haploid products is a necessary (not merely desirable) condition for Track R to produce a safe cell; the ploidy gate at N7 is therefore a hard stop, not a risk to be managed.

6.12 Node N8 — single-cell entropy verification (shared)

The produced cells are verified to be low-entropy (young) relative to the donor's in-vivo HSCs, by the same single-cell entropy pipeline as Track A (Section 5.1). This is the shared endpoint check across the tracks (Section 3.2, Table 2).

6.13 Niche return

The verified product is engrafted autologously (Objective 3 procedures) with the full safety gate.

7. Track C (exploratory, outside registered scope): the centriole-elimination route

Track C offers a second route to the same destination that avoids both the haploid intermediate and meiosis. Its defining feature is that centriole elimination preserves diploidy: the cell is never taken to a haploid state.

7.1 Natural template: centriole removal from the zygote and first blastomeres

The acentriolar state is not an artificial construct; it is a normal stage of early development. In several species the zygote and early blastomeres divide without centrioles, with non-canonical microtubule organisation and de-novo centriole/centrosome formation later in pre-implantation development. The evidence is specific: the mouse pre-implantation embryo is effectively acentriolar with de-novo centrosome formation (Howe & FitzHarris, 2013), and acentriolar mouse embryos form spindles without centrioles in early blastomeres — with an explicit tetraploidy/CIN caveat that feeds directly into the safety gate (Paim & FitzHarris, 2019). Bovine early embryos form centrosomes de novo (Uzbekov et al., 2023), and bovine zygotes assemble dual spindles despite paternal centrosomes, evidencing non-canonical early division (Schneider et al., 2021). In Drosophila, the female-gamete centrosome is eliminated so that the zygote's centrosome comes from the sperm (Pimenta-Marques et al., 2016), and centrioles are dispensable for Drosophila oogenesis yet essential for the first embryonic divisions (Stevens et al., 2007); in C. elegans, centriole elimination during oogenesis begins with loss of the central-tube protein SAS-1 (Pierron et al., 2023), and centrosome elimination during C. elegans oogenesis is cell-cycle-regulated (Kim & Roy, 2006); in parthenogenetic nematodes, functional maternal centrioles are inherited instead (Perrier et al., 2024). Species surveys document the diversity of this biology (Avidor-Reiss et al., 2015; Avidor-Reiss & Fishman, 2019); in human zygotes the sperm contributes an atypical, structurally asymmetric distal centriole alongside the canonical proximal one (Fishman et al., 2018); and meiosis itself eliminates mother and daughter centrioles by distinct mechanisms in starfish oocytes (Borrego-Pinto et al., 2016). Where the mechanism is resolved, natural elimination is staged rather than instantaneous — pericentriolar-material shedding precedes centriole degradation, and the mother and daughter centrioles are eliminated by different routes (Borrego-Pinto et al., 2016; Pimenta-Marques et al., 2016) — which is the direct template for the staged elimination of Track C's C-2. Two natural contexts are thus available as templates: centriole removal during gametogenesis (the Track R template) and centriole absence in the zygote/first blastomeres (the Track C template), both before de-novo synthesis.

7.2 The acentriolar window is feasible, reversible, and guarded

The operational feasibility of an acentriolar window rests on four published lines of evidence. First, acentrosomal division is real and faithful: mouse oocytes assemble spindles by self-organised microtubule-organising centres without centrosomes (Schuh & Ellenberg, 2007), through a conserved liquid-like spindle domain (LISD) machinery dependent on RanGTP and augmin (So et al., 2019). Second, the state is reversible: removal of centrosomes is followed by de-novo assembly, and normal cells pass G1 without centrioles (La Terra et al., 2005; Uetake et al., 2007). Third, the window is pharmacologically accessible: reversible centriole depletion with the PLK4 inhibitor

centrinone arrests normal cells in a p53-dependent G1 hold (without DNA damage) while transformed cells continue to divide (Wong et al., 2015) — this is the molecular basis of the p53 gate. Fourth, the natural barrier is itself a checkpoint rather than an intrinsic lethality: acentriolar mouse embryos survive to mid-gestation, and the observed p53-dependent apoptosis results from prolonged prometaphase, not from the absence of centrioles per se (Bazzi & Anderson, 2014); the prometaphase delay is further controlled by a p38-dependent G1 arrest (Uetake et al., 2007). The window is therefore holdable by p53/p38 blockade, exactly as LERR L4 prescribes.

The mitotic cost of the window is concrete. In centrinone-treated cells that do divide, mitotic fidelity is compromised: mitosis is elongated (roughly 20 minutes in NIH/3T3 cells and up to about an hour in HeLa cells), and the frequency of mitotic errors and cell death rises (Wong et al., 2015). Centriole loss can also push cells toward differentiation rather than toward a reprogramming-competent state. Track C is therefore predicated on a hard feasibility gate: the acentriolar diploid state must maintain mitotic fidelity and reversible quiescence in adult human HSCs within pre-specified error thresholds, or the track is stopped. The natural templates (mouse and bovine zygotes, Drosophila and C. elegans female-gamete elimination) establish that the window exists in vivo, but adult proliferating HSCs are a different, harsher test, and the manuscript does not assume that the window transfers.

7.3 Track C stages

C-1 — Stratify. Autologous cells are stratified by PTM load, centriole age, and entropy baseline (as L1).

C-2 — Safe centriole elimination, diploidy preserved. The centriole is eliminated reversibly by staged PLK4 suppression and controlled degradation of the existing centriole, reproducing the natural elimination templates (mouse/rodent acentriolar zygote; bovine de-novo template; Drosophila female-gamete elimination; C. elegans egg-side elimination). The cell enters a reversible acentriolar diploid state. Staged PLK4 suppression follows the published reversible-centriole-depletion approach (PLK4 inhibition, as in Wong et al., 2015), titrated so that normal cells enter the p53-dependent G1 hold rather than divide, with the p38-dependent arrest (Uetake et al., 2007) available as a second gate; diploidy is verified by karyotype and fluorescence in-situ hybridisation at entry and exit. Quantitative acceptance criteria for the window are pre-specified: chromosome mis-segregation rate ≤ 5% (live-cell imaging or FISH), micronucleus frequency ≤ 10%, viability ≥ 90%, and p53 activation (p21 induction) ≤ 2-fold over baseline, each stable across three independent HSC donors before the track proceeds. These thresholds are framed as non-inferiority to the donor-matched, uncultured HSC baseline: each parameter must fall within a pre-specified equivalence margin of the same donor’s uncultured baseline, rather than being justified against a population

reference, because primary-HSC baseline mis-segregation can itself be a few percent and a population threshold could misclassify. Safety gate: viability ≥ 90%, ploidy intact, no mitotic catastrophe, p53-rollback available.

C-3 — Acentriolar reprogramming window. Partial reprogramming/entropy-lowering is applied in the acentriolar state. The operational rationale is the generic partitioning-mimic (purging aged structures, as gametogenesis does; Goodman et al., 2020); the window's reprogramming competence is tested directly by the totipotency-induction readout of C-4 (N-TOT) and does not rely on the centriole-division-counter hypothesis, which this programme does not adopt (Section 1.5). The C-3 step assumes that acentriolarity is reprogramming-permissive; this is graded [H] in Table 3, and its theoretical motivation overlaps the centriole-division-counter lineage, but its operational test is independent of that model. Safety gate: p53-rollback, genome integrity.

C-4 — Totipotency induction (shared N-TOT). From the acentriolar, reprogramming-primed cell, the totipotent program is activated (ZGA-like / DUX4/DPPA3/Nr5a2; induced-totipotency template), and totipotency is validated.

C-5 — Direct differentiation, no embryo. From the induced totipotent cell, the desired differentiation is obtained directly, to a safe adult HSC. The primary route is defined transcription factors as specified in Section 6.9 (Sugimura et al., 2017; Riddell et al., 2014; Doulatov et al., 2013); centriole transplantation remains an exploratory sub-hypothesis (H4e) only. This is the shared N5 node.

C-6 — Rebuild. Young centrioles are rebuilt de novo (PLK4 → SAS-6 → STIL → CPAP) if and when the mature adult stem cell requires them, with biogenesis validated.

C-7 — Niche return and full safety gate. Autologous engraftment with genome-integrity, ploidy, and tumorigenicity gating (H5).

7.4 Distinctiveness of Track C

Track C differs from Track R in that it reaches the reprogramming-primed state by removing the centriole while keeping the cell diploid (no haploid intermediate, no meiosis, no fusion) and from H4e in that it does not assume an already-totipotent input; it induces totipotency itself via the shared N-TOT node. Its open questions are empirical and precisely stated: is the acentriolar state reversible and non-lethal in adult human HSCs (mitotic-catastrophe risk, mitigated by staged PLK4 suppression and rollback); does centriole removal itself reset the division counter enough to lower entropy (tested by single-cell entropy before/after); and can the desired differentiation be induced reliably from the acentriolar primed state (tested by an empirical induction screen).

8. Track T1: niche rejuvenation (intervention in situ; readouts by aspiration)

Track T1 is the lowest-risk arm and runs in parallel from Year 1. It does not harvest, transform, or return cells; it rejuvenates the environment in which resident HSCs already live, exploiting the fact that a substantial part of the aged HSC phenotype is imposed by the aged niche and systemic environment.

Procedure. (i) **Senolytic clearance.** Senescent niche cells are cleared with the dasatinib–quercetin (D+Q) combination, administered per the published regimen (Xu et al., 2018), with clearance verified by a senescent-cell marker panel (p16/p21 induction and SASP cytokines) in serial aspirates; the target is the accumulation of senescent cells that distort niche signalling and sustain a pro-inflammatory, self-renewal-suppressive microenvironment. (ii) **Niche-signal restoration.** Niche and systemic signals are restored, informed by the demonstration that a young systemic environment rejuvenates aged progenitor cells in vivo (Conboy et al., 2005) and by the partial-reprogramming and systemic-factor literature; the restoring agents (young-plasma-derived factors or a defined niche-signal cocktail) are an open candidate list at registration; the specific factors, routes, doses, and schedules are locked before data collection and recorded in the Stage 1 plan. (iii) **Measurement.** HSC self-renewal, lineage balance, and the aged phenotype are measured before and after intervention. The term “in-situ” applies to the intervention (no harvest-and-return), not to measurement: single-cell entropy requires dissociation, so resident-HSC readouts are obtained by serial bone-marrow aspiration at defined time points, and the programme states this rather than claiming to measure entropy in situ. Where a genuinely in-situ readout is wanted, chromatin-imaging-based proxies (Iáñez Picazo et al., 2025) are reported as a separate, explicitly non-equivalent readout, and the shared N8 measurement standard is maintained for the aspirate-based entropy. **Safety.** Senolytic clearance and signal restoration are the mildest interventions in the programme; the safety gate is nonetheless applied to resident HSC function, and systemic effects are monitored.

Hypothesis. H4g: in-situ niche rejuvenation measurably restores resident HSC function and reduces the aged phenotype. This track serves as a lower-risk parallel and comparator for the deeper tracks.

9. Shared nodes and consolidation of the experimental programme

The shared-node consolidation is introduced in Section 3.2, and Table 2 is the authoritative source; this section states its implications rather than repeating the list.

First, each shared node has one measurement standard and one set of acceptance criteria, so cross-track comparability is maintained by construction. Second, the consortium allocates one responsible expert group per shared node, which bounds the expert burden of the portfolio (Table 4). Third, a shared node that fails its feasibility checkpoint in one track is re-examined in the others before it is judged failed globally, because the input state differs between tracks (for example at N-TOT and N5). Node dependencies and cascading risk are analysed in Section 13.6.

10. Single-cell entropy: measurement methodology

Because entropy is both the selection criterion and the endpoint, its measurement is the methodological backbone of the programme.

Data. Single-cell RNA-seq (scRNA-seq) and single-cell ATAC-seq (scATAC-seq) are generated from freshly sorted cells, with cell-cycle state assigned and carried as a covariate in every model (the association is reported both cell-cycle-adjusted and unadjusted). The computational pipeline is specified in advance with named tools: (i) quality control — removal of low-quality cells, ambient-RNA correction (SoupX), and doublet detection (Scrublet primary, DoubletFinder as sensitivity); (ii) normalisation and variance stabilisation; (iii) integration across donors and batches by Harmony (primary) or scVI (sensitivity), so that donor identity and 10x run-to-run variability cannot masquerade as an entropy difference; (iv) cell-cycle scoring, with cell-cycle state used as a covariate and a G0/G1-restricted sensitivity analysis reported alongside; and (v) cell-type annotation by reference-based mapping against an HSC reference atlas with marker-gene validation, and unsupervised clustering reported as a sensitivity analysis. No G0/G1 restriction is used as the primary strategy, because dye-dilution division tracking requires dividing cells. Computational reproducibility is fixed: software package versions are pinned in a containerised environment (Docker/Conda) with a fixed random-seed policy, and the environment, the pipeline code, and the analysis plan are archived together with the Stage 1 registration. The scATAC component uses established single-cell chromatin-accessibility atlasing (Domcke et al., 2020).

Primary selection metric (age-associated entropy). The selection criterion is age-associated entropy, computed by the primary metric defined here and used consistently across the programme. The primary, pre-registered selection metric is the HSC-specific ageing-clock score: the cell-type-specific clock framework of Buckley et al. (2023) is re-derived on HSC data — the published framework is peer-reviewed, but it was fit to neurogenic brain regions, so the HSC-annotated clock component is re-fit from the Objective 1 atlas, and this re-derivation is itself a pre-registered, gated step (the clock must show age concordance in the atlas before it is used for selection). As an independent cross-check, gene-expression noise within the HSC compartment is quantified with VarID2 (Rosales-Alvarez et al., 2023, peer-reviewed), which shows that

HSCs carry the lowest noise of the haematopoietic hierarchy and that noise rises with differentiation and with age. The manifold-deviation entropy of Yang et al. (2026) is an exploratory secondary metric, not a selection criterion: it is a preprint whose formalism has not been peer-reviewed or validated on HSC data, so it is computed in parallel and may be promoted to a selection criterion only after it passes the validation block and the age-concordance check in the pilot; until then it is reported alongside the primary metric but does not drive selection. The primary contrast for selection is the ageing-clock score (with VarID2 as the cross-check), fixed before sorting; where the manifold score is reported, it is labelled exploratory. At registration, neither candidate metric is pre-designated as primary in a way that creates a single point of failure: the operational selection criterion is whichever candidate — the re-derived clock or the manifold score — passes the pre-registered validation block (age concordance on hold-out data and VarID2 concordance), and if neither passes, selection is deferred and reported. The manifold score has existing haematopoietic age-association evidence (Yang et al., 2026); the clock has a peer-reviewed framework; both are evaluated on equal pre-specified criteria. A split-reference design is enforced: the donors used to build the reference manifold (or to fit the HSC clock component) are independent of the donors used to validate selection; if any overlap exists, H2 is automatically downgraded to exploratory and reported as such. A leave-one-donor-out sensitivity analysis re-builds the reference and re-tests the selection signal excluding each donor in turn.

Operational definition of the primary metric. Concretely, manifold-deviation entropy for a cell x of type T is computed in four steps: (i) a reference set of young, functionally validated HSCs from the same donor pool defines a reference transcriptomic manifold, constructed by diffusion-map or PCA embedding of the log-normalised expression matrix, where the reference set is built specifically on functionally validated long-term HSCs (LT-HSC: Lin−CD34+CD38−CD45RA−CD90+CD49f+), not on the whole CD34+ pool, because the HSC compartment is functionally heterogeneous; “functionally validated young” is defined by serial-transplantation capacity (multilineage reconstitution maintained to a secondary transplant at ≥ 16 weeks) or an equivalent functional criterion explicitly distinct from the primary H3/H4 engraftment endpoint, so that the reference definition and the outcome measure are not the same assay, and, where functional validation is unavailable, by donor chronological age below 25 years with the substitution recorded as a stated limitation; the pilot computes the entropy score under both the chronological-proxy and the functional-LT-HSC reference definitions and reports their Spearman ρ, so that the choice of reference cannot silently determine the result; the bias of this chronological-age proxy is unknown, so the pilot reports both the proxy-based and any functional-based reference definitions and reports any discrepancy between them; pre-registered handling of reference-set discordance: if the two reference definitions are discordant (Spearman $\rho < 0.6$) on the same cells, the functional-based definition governs when it is available, otherwise the proxy is used with

the discordance reported as a methods finding, and if functionally validated LT-HSCs are unavailable in the pilot, the proxy's bias is quantified by the age-concordance check against the full donor-age gradient (validation block); (ii) each query cell is projected onto that embedding; (iii) the cell's score is the normalised distance (Mahalanobis or geodesic) from the reference manifold in expression space, scaled so that the reference cells have mean 0 and unit standard deviation; and (iv) the score is validated against the ageing-clock and VarID2-noise measures (validation block below) before use. Parameter choices are fixed in the analysis plan with stated sensitivity ranges: PCA dimension chosen by the elbow criterion (50–100 components); diffusion time fixed through the reference embedding; distance metric Mahalanobis with regularised covariance as primary and geodesic as a sensitivity analysis; and kNN k = 20 with range 10–40 for the graph-based variants. The pilot reports every primary analysis under the primary parameter set and under the sensitivity range, so that conclusions do not rest on a single parameter choice. The sensitivity protocol is pre-registered explicitly: at least three alternative parameter combinations (kNN k = 10, 30, 40; PCA dimension 30, 75, 100) are run, and a primary inference is judged robust only if its direction is identical across all combinations; any divergence is reported rather than resolved post hoc. A negative control is included: the same pipeline applied to a set of housekeeping genes that are not expected to change with age must not produce a spurious age-associated entropy signal, and any such signal invalidates the metric until the cause is identified. A positive control is included: HSCs cultured under a known entropy-raising condition (for example, hydroxyurea-induced replicative stress) must show the expected increase in age-associated entropy, confirming that the pipeline can detect a known signal; without a passing positive control, the metric is not used for selection. A culture-artefact negative control is included: the entropy of fresh, uncultured HSCs is compared against HSCs cultured for 24 h without division (cytokine starvation), with a pre-specified equivalence margin ($|\Delta\text{entropy}| \leq 0.2$ SD units, two one-sided tests), to separate culture-induced drift from division-linked entropy. A lag risk is acknowledged: a cell that is functionally aged but not yet transcriptionally disordered may score as low-entropy, so manifold-deviation entropy can lag functional ageing; the validation block's age-concordance check and the functional endpoints of H3/H4 are the controls for this lag. For the ageing-clock route, the score is the cell-type-specific clock prediction of age applied to HSC-annotated cells. Conceptually, the operational construct is the deviation of a cell's transcriptome from the HSC reference manifold; the peer-reviewed, re-derived clock is the pre-registered proxy for that construct, and the manifold score is the construct-validity measure. The pilot's central methodological task is to establish whether the two operationalize the same construct (concordance); only then is the selection criterion promoted to the direct manifold measure. The published cell-type-specific clock framework (Buckley et al., 2023) was fit to neurogenic brain regions, so the HSC-annotated clock component is re-derived from the Objective 1 atlas rather than

assumed to transfer. The re-derivation uses a hold-out donor set or nested cross-validation, so that the clock is never validated on the same donors that are later selected on; the age-concordance and VarID2-concordance thresholds are evaluated on the hold-out set before the clock is used prospectively.

Secondary, potency-flagged metric. Signalling entropy (Teschendorff & Enver, 2017; network-theoretic formalism in Teschendorff et al., 2014) is computed only as a secondary analysis. It measures differentiation potency — high in undifferentiated cells, low in terminally differentiated cells — and is therefore never used as the selection criterion. Where reported, it is labelled as a potency measure, and a cell-cycle- and potency-adjusted analysis is presented to show that selection on age-associated entropy does not merely recover potency differences. This separation is structural rather than cosmetic: using signalling entropy as the selector would select for low potency, the opposite of the programme's aim.

Selection logic. The low-entropy fraction is defined prospectively as the lowest decile of the age-associated-entropy distribution of the donor's HSC pool, with the threshold fixed before sorting. Selection is validated by index-sorted single-cell re-measurement of the sorted product, and by demonstration that the selected fraction is lower-entropy than donor-matched in-vivo HSCs (H2). Pre-specified contingency for the potency axis: if the selected lowest-decile age-associated-entropy fraction is also in the lowest quartile of signalling (potency) entropy, the fraction is flagged as potentially quiescent or undifferentiated. In that case the functional engraftment assay (H3/H4) is the decisive test; a failure to reconstitute multilineage chimerism would indicate that low age-associated entropy alone is insufficient, and the selection criterion would be revised to include a minimum signalling-entropy floor. This contingency is pre-specified in the analysis plan rather than decided after the data are seen.

Stability. Selected cells are re-measured after culture and after engraftment to test whether the low-entropy state is retained or reverts.

Automation (H6). The ARGUS platform automates microscopy, single-cell entropy scoring, quality control, and process monitoring, providing an auditable log for every cell product and every ladder stage.

Validation of the metric. The entropy metric is validated before it is used as a selection criterion, on four grounds: (i) age concordance — the metric must increase with donor age within the HSC compartment of the Objective 1 atlas; note that the age–entropy association is contested (a multi-tissue analysis found no evidence of increased transcriptional noise with age, Ibañez-Solé et al., 2022), so age concordance is a pre-registered validation target specific to the HSC compartment, not an assumed fact; (ii) cell-cycle separation — the metric must not be dominated by cell-cycle position, tested by comparing entropy within G0/G1 against the full population (a validation check only;

the primary analyses carry cell-cycle state as a covariate); (iii) reproducibility — technical replicates of the same cells must give intra-class correlation ≥ 0.95, a threshold set by published single-cell reproducibility standards and re-validated on pilot data before use; and (iv) cross-metric concordance — the manifold score and the ageing-clock score must be concordant on the same cells (both age-associated measures are reported as standard), while the potency metric is validated separately (Section 10, secondary metric). Only after these four checks pass is the metric used for prospective selection. Pre-registered discordance rule: if the manifold and ageing-clock scores are discordant (Spearman $\rho < 0.6$ on the same cells), the selection arm is deferred — neither metric is used for prospective selection until the discordance is resolved on independent (hold-out) data — and the discordance is reported as a methods finding rather than resolved by choosing the more favourable metric post hoc.

11. Safety gate (H5): genome integrity and tumorigenicity

The safety gate is a co-primary endpoint of every track and is deliberately conservative. Acceptance criteria are defined a priori: no increase in structural or numerical chromosome aberrations beyond a predefined background; no oncogenic mutation signature introduced by the manipulation; no teratoma or tumour formation in the 12-week subcutaneous assay; no clonal-haematopoiesis expansion beyond age-matched background (Jaiswal et al., 2014). Immunogenicity of the product is also gated. Autologous iPSC-derived cells are not inherently immunologically inert: de-novo mitochondrial-DNA mutations acquired during reprogramming and prolonged culture generate neoantigens that can provoke strong, MHC-restricted immune responses and transplant rejection in otherwise autologous settings (Deuse et al., 2019). The screen is tiered by manipulation. Minimal-manipulation products (selection followed by immediate transplant, without extended culture) are not subject to a mandatory mitochondrial screen; mitochondrial sequencing is then an exploratory readout only. Extended-culture products (reprogramming, differentiation, or selection with expansion) are subject to mandatory deep mitochondrial sequencing, with the release threshold pre-specified: no homoplasmic or near-homoplasmic (allelic fraction > 90%) de-novo mtDNA variant above background, where the background is defined as the donor-matched, pre-manipulation sample of the same product lineage rather than a population reference (aged-donor baseline heteroplasmy can be substantial), and a variant is reportable only if its allelic fraction exceeds the donor's baseline by a pre-registered margin (at least a doubling of the donor's baseline heteroplasmy at that position, or > 10% absolute allelic fraction, whichever is larger), and a predicted neoantigen load below a threshold informed by Deuse et al. (2019); the threshold and its derivation are archived with the Stage 1 registration. Boundary statement: the division-tracking culture of the pilot (72–96 h, CFSE/PKH26) is classified as minimal manipulation for this protocol, and mitochondrial sequencing is not mandatory for that step but is performed as an

exploratory readout; if any pilot product shows a de-novo mtDNA variant above background, the boundary is re-evaluated before the full study. Brief OSK pulses (1–3 days) are classified as borderline rather than minimal manipulation: they involve transfection reagent, synthetic mRNA, and metabolic stress, so mitochondrial sequencing is performed on all induced products regardless of culture duration, and the release threshold is applied. Serial transplantation is used as the functional test of long-term safety and self-renewal. The design incorporates the known aneuploidy risks of the deep tracks — achiasmate meiosis (N2/N7), haploid intermediates (N-HAPLO), and the tetraploidy/CIN caveat of acentriolar embryogenesis (Paim & FitzHarris, 2019) — as monitored, gated quantities rather than as after-the-fact concerns.

12. Statistical design, endpoints, and power

All primary endpoints are pre-registered with the falsification criteria of Section 2. The primary, pre-specified power statement concerns the paired entropy contrast — the within-donor difference between the selected (lowest-decile) fraction and the donor-matched in-vivo HSCs — analysed with linear mixed-effects models using the full random structure — a random intercept for donor, a random slope for division within donor, and a nested donor-by-division-peak term for the non-independence of cells sharing a donor and a division peak — controlling for cell-cycle state and donor age. For H1, a mediation analysis is pre-registered: the total effect of division history on entropy (unadjusted) and the direct effect (adjusting for cell-cycle state) are both reported, with the total effect pre-specified as the primary estimand; if the direct effect is zero while the total effect is significant, the coupling is cell-cycle-mediated, which is a finding rather than a nuisance to be removed. For a paired difference of Cohen's d = 0.5 at two-sided $\alpha = 0.05$ and within-donor correlation r = 0.5, the paired-difference formula $n \approx (z_{1-\alpha/2} + z_{1-\beta})^2 \cdot (1 - r)/d^2 + 2$ gives n ≈ 23 donors at 90% power; this is an indicative calculation only. A sensitivity power analysis is reported across plausible effect sizes at the same r and 90% power: n ≈ 133 (d = 0.2), n ≈ 60 (d = 0.3), n ≈ 23 (d = 0.5); because no published estimate anchors the effect size, the smallest of these that the programme would fund (d = 0.3, n ≈ 60) is the practical planning value, and a pilot-derived d below 0.3 re-baselines the programme to Track T1 rather than committing to a prohibitively large study. The within-donor correlation r = 0.5 is a conservative assumption to be estimated in the pilot; no published estimate exists for this specific correlation. The pilot (n = 12, Section 5.7) is not a confirmatory test of H1; it provides the first empirical estimate of d and its variance for HSC entropy contrasts, and the confirmatory sample size for the full study is derived from that estimate by a precision-based (assurance) approach rather than fixed at any assumed d. The pilot is not used to decide scaling. Its role is to estimate variance components and to confirm feasibility; the full-study sample size is computed from the pre-specified smallest effect size of interest (SESOI) by power analysis, not from the pilot's observed d. The pilot's d is reported but does not

gate the full-study n, except through the decision boundary of Section 12 (a pilot-derived d below 0.3 re-baselines the programme to Track T1). If the pilot estimate is substantially below the assumed d = 0.5, the protocol is amended and re-registered rather than continued under the original power statement; a sequential-analysis framework is pre-registered to formalise this decision. The SESOI (|β| ≥ 0.1 SD units per division) is set provisionally by convention, but its final value is justified empirically from the within-donor, within-division-peak variance estimated in the pilot, rather than from the Cohen benchmark alone, and the interpretive threshold is updated in a re-registered amendment if the pilot variance shows that 0.1 SD is within technical noise. A pre-specified decision boundary is set: if the pilot-derived d is below 0.3, the programme re-baselines to Track T1 rather than scaling up; between d = 0.3 and d = 0.5, the sample size is re-derived from the estimate; at or above d = 0.5, the pre-registered design stands. Decision tree for a null H1: if the coupling regressions are null, the cause-targeting rationale for induction (2b) is removed and the programme re-baselines to Track T1; if Track T1 is also null, the programme's premise (that niche and stem-cell rejuvenation measurably restores function) is falsified and is reported as such. These outcomes are planned, not concealed. Gate 1 does not use the pilot's H1 p-value as a pass/fail criterion: with n = 12 the pilot cannot distinguish "no coupling" from "underpowered" (a null H1 p-value is expected even under a true effect). The scaling decision rests on the pilot-derived variance and the pre-registered effect boundary (a pilot-derived d below 0.3 re-baselines the programme to Track T1); otherwise the full-study power is re-derived from the pilot variance and the programme proceeds. The effect size d = 0.5 is a pre-registered assumption, not a literature-derived value — no published estimate anchors the division-rate–entropy effect size in HSCs — so it is treated as provisional; the pilot (Section 5.7) estimates d and its variance, and the full-study sample size is re-derived from that estimate by a precision-based (or Bayesian design-analysis) approach rather than fixed at d = 0.5. In the pilot, the random structure is simplified for estimability with n = 12 donors (a random intercept for donor, with a random slope for division added only if the pilot data support it); the full nested structure is reserved for the full study. The design enrols ≥ 40 donors per age group, which covers the paired contrast (n ≈ 23) with margin and supports the donor-level coupling regression (H1) at 90% power for r ≥ 0.4. For the cell-level H1 model, the detectable association depends on the number of cells per division peak per donor: with ≥ 5,000 cells per donor per peak (Section 5.7.3) and n = 40 donors per age group, the design provides ≥ 90% power to detect a per-division entropy increase of ≥ 0.1 SD units (a random-slope coefficient of that magnitude). The pilot estimates the within-donor variance components and re-derives the required cell count per peak for the full study. Power for the cell-level H1 model is computed on the donor-level variance component, not on the cell count: because cells from the same donor and division peak are correlated, the effective sample size is the number of donors (and of donor-by-peak

clusters), and the thousands of cells per peak improve precision within a cluster without inflating the donor-level power; the stated ≥ 90% power for a per-division increase of ≥ 0.1 SD units is therefore based on the donor-level ICC. The power is reported across assumed donor-level ICC values (0.3 and 0.5): a higher ICC (stronger donor clustering) reduces the effective sample size, and the reported ≥ 90% figure assumes ICC ≈ 0.5; if the pilot estimates a higher ICC, the required n is re-derived accordingly. Missing-data handling is pre-specified: a donor that yields no cells in a required division peak (for example, no ≥ 3-division peak) is excluded from analyses that require that peak, with the exclusion recorded and the affected analysis reported; no missing peak is imputed. A sequential-analysis framework is pre-registered with an O'Brien–Fleming alpha-spending function, with an interim analysis at 50% of planned enrolment and a final analysis at the full sample; stopping rules are pre-specified for efficacy and futility. The engraftment arms of n = 8 per arm are a proof-of-concept size, not a powered efficacy test: a two-proportion test at n = 8 per arm has only approximately 40% power to detect a doubling from 40% to 80% at $\alpha = 0.05$, and this is acknowledged; the powered efficacy comparison is deferred to the full study. For the directional decision rule of Section 2 (H3), the relevant quantity is a non-inferiority test (selected no worse than unselected, margin −10 percentage points): at n = 8 per arm with an assumed true difference of zero and a chimerism standard deviation of about 20 percentage points, the power is approximately 60%, which is reported here so that the rule's operating characteristics are explicit. The comparison standard for functional benefit is the published partial-reprogramming benchmark (Ocampo et al., 2016; Lu et al., 2020; Sahu et al., 2024); the programme claims superiority only if the entropy-selected/induced product beats this comparator on the pre-registered readouts with the safety gate intact. Multiple-testing control uses the Benjamini–Hochberg false-discovery-rate procedure at $q = 0.05$ across the primary endpoint families (entropy contrasts, functional engraftment readouts). Blinding and randomisation: sample processing and computational analysis are performed by analysts blinded to donor age group and to treatment arm; the randomisation schedule is generated before recruitment and archived with the Stage 1 registration, with a pre-registered unblinding rule. Because eleven primary hypotheses are pre-registered (H6 excluded as an engineering criterion), a worst-case Bonferroni threshold ($\alpha \approx 0.0045$) is reported as a sensitivity analysis, and the power statement is re-checked against it at the analysis-plan stage. The re-check is stated here: at the two-sided Bonferroni threshold $\alpha \approx 0.0045$ with $d = 0.5$ and $r = 0.5$, the paired design requires $n \approx 30$ donors for 80% power, which the ≥ 40-donor enrolment covers; the sensitivity analysis is therefore power-consistent, not merely reported. The FDR family is pre-registered hierarchically: the confirmatory family comprises H1, H2, H3, H4 and H4b (induction is the production route, so H4b is confirmatory rather than exploratory), and the exploratory family comprises H4c, H4d, H4e, H4f and H4g, with FDR control applied within each family

rather than across all eleven. The hierarchical dependency between H4c and H4b is acknowledged: partitioning-mimic (H4c) is a prerequisite for the induction route (H4b) in the production logic, so the families treat them as separate endpoints but a null H4c is reported as a constraint on H4b's interpretation rather than as an independent null. A failure at any gate is reported as a falsification rather than silently repaired; the architecture is structured so that negative results surface at the node where the evidence is missing.

12.1 Timeline and decision gates

The programme is staged so that high-risk tracks are entered only through gates opened by lower-risk results. Years 1–2: Track A core (coupling, selection) and Track T1 run in parallel; the coupling result (H1) determines whether induction (2b) is cause-targeted or generic. Gate 1 (end of Year 2): H1 and H2 must pass, or the programme re-baselines to T1 alone. Years 2–3: induction (2b) and partitioning-mimic (2c). Gate 2 (end of Year 3): H4b or H4c must pass with the safety gate intact, or the deep tracks are not advanced past feasibility. Years 3–5: Track C (C-1–C-7) and, only if the acentriolar window is confirmed permissive, Track R (N1a–N8). Track R carries no committed timeline: it is entered only after the achiasmate-meiosis feasibility gate (euploid achiasmate products in a model organism) is passed, which may take considerably longer than the programme horizon and is stated as such rather than scheduled. Each node has a feasibility checkpoint; a node that fails its checkpoint is reported and the track is stopped rather than silently repaired. ARGUS (H6) is developed continuously and its fidelity thresholds are evaluated at every gate.

12.2 Registration and reporting

Registration and reporting. The primary analyses, entropy thresholds, and falsification criteria are pre-registered before data collection, and the analysis code — including all model specifications, entropy-threshold definitions, and FDR family assignments — is frozen and deposited with a timestamp that precedes the first sample. Negative and positive results are reported symmetrically, and all cell products, ladder logs, and entropy computations are archived for re-analysis. Method preprints accompany each completed node, so the programme publishes its failures as well as its successes.

13. Discussion

13.1 The nodes are individually supported and the tracks share their procedures

The central design claim is that the multi-track architecture is not additive but shared: six procedures recur identically across tracks, so the programme is a single coordinated pipeline with one validated implementation per shared node. Each node's evidence base is cited above and verified; the two deep tracks are complementary in risk

(haploid-mediated vs. diploid-preserving), and the two low-risk tracks (A core, T1) are implementable in the first years while the deep tracks are being de-risked.

13.2 Principal weaknesses and how the design addresses them

(1) Division-rate–entropy coupling is assumed, not established. The entire selection logic rests on a coupling that has not been directly tested in HSCs. The design responds by making the coupling the first experiment (Objective 1) and by ensuring that induction (Objective 2b) is retargeted at its causes if it is found.

(2) Entropy may reflect cell-cycle state rather than youth. Cell-cycle state is carried as a covariate in every model, the association is reported adjusted and unadjusted, and a G0/G1-restricted sensitivity analysis is reported alongside.

(3) The deep tracks pass through fragile intermediates. Haploid cells spontaneously diploidise; achiasmate meiosis is normally lethal; the acentriolar window is a checkpoint-held state. Each of these is a named node with an explicit failure condition and mitigation (N-HAPLO, N-MCHK, C-2/p53-gate), and each is gated rather than assumed.

(4) Surface youth markers may be unstable. The fallback (direct index-sorted entropy selection on fresh cells) is specified in advance.

(5) The humanised-mouse niche may not model human HSC self-renewal fully. The complementary in-vitro niche-coculture and transcriptional-clock readouts are specified.

(6) N5 (the differentiation mechanism) is the least-supported deep node. It is honestly labelled as the key falsifiable experiment, with a defined fallback to empirically mapped inductors.

13.3 Comparison with existing approaches

The partial-reprogramming field (Ocampo et al., 2016; Lu et al., 2020; Sahu et al., 2024) achieves markers of rejuvenation but measures them at bulk or population level and does not select on entropy; parallel EU-funded programmes are pursuing HSC partial reprogramming with defined-factor delivery, and the present programme's differentiator is the use of age-associated entropy as the selectable endpoint and the autologous-return architecture rather than reprogramming alone. The IVG field (Ishiguro et al., 2020; Sagi et al., 2016; Pierson et al., 2019) establishes the germline and haploid systems that Track R depends on, but does not combine them with recombination blockade, autologous fusion, and entropy-verified differentiation. The centriole literature (Howe & FitzHarris, 2013; Wong et al., 2015; Bazzi & Anderson, 2014; Pimenta-Marques et al., 2016) establishes the acentriolar window that Track C uses, but has not used it as a therapeutic route to adult stem cells. The senolytics and parabiosis literature (Xu et al.,

2018; Conboy et al., 2005) establishes Track T1's interventions. The contribution of the present programme is the integration: entropy as the selectable and inducible endpoint, autologous return as the therapeutic operation, and the shared-node architecture that makes the integration experimentally tractable.

13.4 Ethical and regulatory considerations

The programme is designed to avoid the use of embryos: totipotency is induced in vitro and differentiation proceeds directly, without the destruction of an embryo. The human relevance of the deep tracks is staged behind animal validation. Two additional ethical dimensions are treated substantively. First, the totipotency and PGCLC work involves germline-competent cells; its permissibility is jurisdiction-dependent and is assessed against the relevant legal frameworks of the host institutions before any human material is used, with explicit documentation of the applicable boundaries on germline modification. Second, totipotency work carries teratoma and chimerism risk if cells are delivered inappropriately; the safety gate therefore includes, beyond the 12-week subcutaneous teratoma assay, strict containment during culture, release criteria that exclude residual undifferentiated totipotent cells, and a pre-specified plan for detection and management of accidental chimerism in the animal model. All manipulations of human cells fall under standard cell-therapy and genome-integrity regulation; the safety gate (Section 11) is intended to be stricter than the minimum regulatory requirement. Specific commitments are made here: (i) all donor material is obtained under informed consent for the stated research purpose, with explicit disclosure of the reprogramming and genetic-manipulation steps; (ii) any genetic or epigenetic manipulation of human cells is reviewed and approved by the competent genome-editing and gene-therapy oversight bodies before initiation, and only somatic, non-heritable alterations are pursued; (iii) PGCLC and totipotency work is conducted under the relevant stem-cell and embryo-research guidelines of the host institutions, and no human embryo is created or destroyed at any point. A boundary statement is included for Track R: PGCLCs are not embryos, but the fusion product of two induced gamete-like cells is a zygote-like entity; the programme defines the point at which an entity is treated as embryo-like for ethical and regulatory purposes as the formation of a diploid product with a functional centrosome — the point at which an independently dividing, developmentally competent cell exists, consistent with the N4 centriole node — and commits to completing all Track R operations in non-developable cell states before that point and not proceeding beyond it under the current approvals; the boundary is framed in line with the ISSCR Guidelines for Stem Cell Research and Clinical Translation. (iv) biosecurity review covers the recombination-blockade and fusion technologies to prevent dual-use misuse; and (v) all single-cell and genomic data are managed under the applicable data-protection and governance frameworks. (vi) Every autologous product that passes through reprogramming or prolonged culture is screened for de-

novo mitochondrial-DNA mutations and predicted neoantigens (Deuse et al., 2019), and only products below the pre-specified threshold are released. Residual totipotent cells are detected by a dual marker panel (LIN28A and DPPA3, or an equivalent pair) on at least 10,000 cells per product, with a release threshold of fewer than 0.01% positive cells; products above the threshold are discarded, not further differentiated. This screen applies to every product that passes through a totipotency-induction or reprogramming step, including Track A products after OSK pulses and recovery, not only to deep-track products. All animal work follows the 3Rs (replacement, reduction, refinement): the humanised-mouse engraftment is the minimum animal model required for the niche question, cohort sizes are pre-specified to avoid redundant animals, and endpoints are chosen to minimise distress. No claim of whole-body rejuvenation is made; the scope is functional young haematopoiesis from autologous cells.

13.5 Open questions that the programme is designed to answer

Is the division-rate–entropy coupling causal or a correlate of donor age? Are youth markers exportable to clinical surface panels? Is the low-entropy state stable after selection, culture, and engraftment? Does autologous return improve long-term haematopoiesis beyond 16 weeks? Can the principle extend beyond HSCs to muscle satellite cells and mesenchymal stem cells? Is the acentriolar window a permissive state for totipotency induction in adult human cells? Each question is attached to a node with a measurable output, so each has a defined way of being answered — or falsified.

13.6 Systematic evidence assessment of the nodes

To make the meta-analysis of the architecture explicit, every node is assessed on the same evidence scale used in the hypotheses ([E] established, [I] inferred, [H] hypothetical), with the supporting references. Table 3 summarises the assessment; Table 4 compares the tracks by risk, TRL, timeline, and evidence strength.

Table 3. Evidence assessment of the technical nodes.

Node	Grade	Context of evidence	Key evidence
N8 single-cell entropy	[I] method (preprint/transfer), [H] as selectable marker; direction caveat addressed	human/mouse single-cell; HSC not yet validated	Teschendorff & Enver (2017); Buckley et al. (2023); Yang et al. (2026)

Node	Grade	Context of evidence	Key evidence
Division-rate–entropy coupling	[I] (mechanistic prerequisite established via division counting; the coupling itself is untested)	— (to be tested in this programme)	Bernitz et al. (2016); Qiu et al. (2014); H1, this manuscript
Partial reprogramming (OSK)	[E]	mouse, in vivo/ex vivo; human iPSC in vitro	Takahashi & Yamanaka (2006); Warren et al. (2010); Ocampo et al. (2016); Lu et al. (2020); Sahu et al. (2024)
Germline quality control / partitioning	[E]	yeast, C. elegans, mouse germline	Goodman et al. (2020); Samaddar et al. (2021); Xu et al. (2021); Lv et al. (2020); Feng et al. (2026); Valenzuela-Villatoro et al. (2026); Zhang et al. (2026)
N1a PGCLC induction	[E] in mouse (end-to-end); [I] human specification; [H] adult HSC context	mouse PGCLCs → oocytes → offspring; human PGCLC specification	Hayashi et al. (2012); Pierson et al. (2019)
N1 meiosis	[E]	mouse germ cells	Baltus et al. (2006); Ishiguro et al. (2020)

Node	Grade	Context of evidence	Key evidence
entry (STRA8/ MEIOSIN)			
N2 recombination block + N-MCHK	[E] mechanisms; integration [H] and hard-gated	mouse/yeast meiosis	Kawashima et al. (2023); Rinaldi et al. (2017); Bai et al. (2024); SPO11/ATM literature (Section 6.3–6.4)
N-HAPLO haploid stabilisation	[E] in human/mouse ESC; [H] in adult HSC context	haploid embryonic stem cells (mouse, human)	Sagi et al. (2016); Edwards et al. (2021)
N3 gamete fusion → diploidy	[E] method, [H] as therapeutic step	cell-fusion/hybrid biology (non-meiotic)	fusion/hybrid biology (Section 6.6)
N-ZGA / N-TOT totipotency	[E] factors, [H] induction in this context	mouse/human embryo, induced-totipotency lines	Hendrickson et al. (2017); induced-totipotency literature
N5 differentiation (operational: defined TF; exploratory:	[H] functional adult-HSC output (replication contested); [I] in pluripotent	human pluripotent → HSPC; mouse blood → iHSC	Sugimura et al. (2017); Riddell et al. (2014); Doulatov et al. (2013); Section 6.9

Node	Grade	Context of evidence	Key evidence
centriole transplant)	systems; [H] centriole-transplant sub-hypothesis (H4e)		
N4 de-novo centriole biogenesis	[E]	human/rodent cell lines, embryos	La Terra et al. (2005); Uetake et al. (2007); Wong et al. (2015)
Acentriolar window (Track C) — existence (reversible, checkpoint-held)	[I] in adult HSC context (evidence from oocytes, embryos, cell lines)	oocytes, pre-implantation embryos, cell lines; not adult HSCs	Schuh & Ellenberg (2007); So et al. (2019); Wong et al. (2015); Bazzi & Anderson (2014); Howe & FitzHarris (2013); Paim & FitzHarris (2019)
Acentriolar window (Track C) — reprogramming competence	[H] (untested in adult HSCs)	— (to be tested in this programme)	Section 7.3 (C-3); testable by the C-4 totipotency readout
N7 genome integrity gate	[E] methods	human cytogenomics practice	Jaiswal et al. (2014) and cytogenomics practice
Senolytic	[E]	mouse; clinical senolytics trials	Xu et al. (2018); Conboy et al. (2005)

Node	Grade	Context of evidence	Key evidence
clearance / niche restoration (T1)			

Note on Table 3: evidence is assessed at the level of the operation, and the table does not equate evidence across species or cell types. Where the supporting data come from a different context — for example, acentriolar-window evidence from oocytes and pre-implantation embryos, ageing-clock evidence from brain, or IVG/haploidy evidence from mouse — the extrapolation to adult human HSCs is treated as a separate, unverified assumption and is flagged in the corresponding node section rather than absorbed into the [E] grade. The clearest extrapolations are: oocyte/embryo → adult HSC (acentriolar window), brain → HSC (ageing clock), and mouse → human (PGCLC, haploidy, imprinting); their extrapolation distance is large, moderate, and moderate-to-large, respectively, and this distance is carried in the Context column of Table 3 rather than being absorbed into the grade. This table is a narrative evidence assessment, not a formal meta-analysis: quantitative heterogeneity (I^2) and risk-of-bias scores are not estimable for these single-node qualitative claims, no meta-analytic pooling is performed, and none is claimed.

Node dependencies and cascading risk. The architecture is not a collection of independent nodes; some nodes are upstream of others, so a failure cascades. In Track A, the coupling node (H1) is upstream of induction design (2b) and of the selection claim (H2): a null coupling result does not kill selection (selection can still be tested) but removes the cause-targeting rationale for induction. In Track R, the chain is serial: N1a (PGCLC) → N1 (meiosis) → N2×N-MCHK (achiasmate meiosis) → N-HAPLO → N3 → N-ZGA/N-TOT → N5; a failure at N2×N-MCHK (the empirically weakest link, given the checkpoint evidence above) makes every downstream R node unreachable, which is why Track R is gated at that point and not committed. In Track C, C-2 (elimination) is upstream of C-4 (totipotency induction): if the acentriolar window is not reprogramming-competent (graded [H]), C-5 and C-6 are unreachable, and the track stops at C-4. This dependency structure is the reason the feasibility gates are placed where they are.

Table 4. Track decision analysis (risk, TRL, timeline, evidence strength).

Track	Starting TRL	Timeline	Principal risk	Evidence strength	Role
A core (selection)	TRL 3–4	Years 1–2	coupling absent / markers unstable	high (all parts established)	primary, first

Track	Starting TRL	Timeline	Principal risk	Evidence strength	Role
A (induction 2b, partition-mimic 2c)	TRL 2–3	Years 2–4	entropy not reducible	medium–high	primary
T1 (in-situ niche)	TRL 3–4	Years 1–2	niche not the limiting factor	high	parallel, low risk
C (centriole elimination)	TRL 1–2	Years 3–5	acentriolar window not permissive	medium (window established; totipotency route [H])	exploratory, gated
R (meiotic partition)	TRL 1	gated; no committed timeline	achiasmate meiosis non-viable	medium (nodes [E], integration [H])	exploratory; entered after model-organism gate

We treat the distinction between established and hypothetical evidence explicitly: the only node that is both essential and unaudited is the division-rate–entropy coupling itself, which is why it is the first experiment and the first gate. The deep tracks rest on individually established nodes whose *integration* is hypothetical; the table makes explicit which combination must be de-risked before the deep tracks can be advanced.

Table 5. Risk register (principal programme risks, likelihood, impact, mitigation).

Risk	Likelihood	Impact	Mitigation
Division-	moderate	high (selection	Gate 1; induction

Risk	Likelihood	Impact	Mitigation
rate–entropy coupling absent		logic fails)	becomes cause-agnostic; T1 continues
Youth markers unstable in culture	moderate	medium	index-sorted entropy selection on fresh cells
Achiasmate meiosis non-viable	high	high (Track R)	N-MCHK titration; Track C unaffected
Spontaneous haploid diploidisation	high	medium (Track R)	N-HAPLO stabilisation; continuous ploidy monitoring
Acentriolar window lethal in adult HSCs	moderate	high (Track C)	staged PLK4 suppression; p53/p38 gates; rollback
Safety-gate failure	low–moderate	critical	product not released; parallel tracks provide fallback
Automation fidelity below threshold	low	medium	H6 thresholds evaluated at every gate; manual fallback

13.7 Translational significance

The programme's target (a young, autologous, non-immunosuppressed cell product) addresses a concrete clinical need. Current allogeneic haematopoietic transplantation is limited by donor availability, graft-versus-host disease, and the immunosuppression that accompanies it; autologous transplantation is limited by the age of the graft. An autologous product whose entropy is measurably lower than the donor's in-vivo HSCs would, if functional, remove both limits at once. The autologous claim is stated with one qualification: cells that have been reprogrammed or expanded may acquire de-novo mitochondrial mutations and neoantigens (Deuse et al., 2019), so "no immunosuppression" is conditional on passing the immunogenicity screen of Section 11 rather than an unconditional property of the approach. The same architecture is portable:

the selection/induction logic (Track A) does not depend on haematopoiesis, and the entropy endpoint is measurable in any dividing stem-cell system (muscle satellite cells, mesenchymal stem cells), so the programme is designed as a first instance of a general operation rather than a blood-only fix.

13.8 The strongest counterarguments, and the design's response

(a) "Entropy is a correlate, not a cause." If low entropy does not confer function, selection confers no benefit. The design answers this empirically: H3/H4 test function, and the comparator is the best existing rejuvenation benchmark. If the selected product fails functional readouts, H4 is falsified and the induction arm is re-targeted — the programme is not committed to the hypothesis being true. Low age-associated entropy (and low noise) is treated as a candidate marker whose functional validity is decided by the functional endpoints (H3/H4), not assumed from the metric alone; the validation block's age-concordance and the engraftment test are the arbiters. A concrete opposing scenario is stated: low age-associated entropy could select quiescent, non-dividing HSCs rather than functionally young ones. The potency contingency (Section 10) and the functional engraftment endpoint (H3/H4) are the specific tests that would discriminate these; a null or reverse functional outcome is reported, not hidden.

(b) "The deep tracks are not established at scale." This is a real limitation, and we treat it as one: Track R is conditional, not parallel, and is entered only after Track C confirms a permissive acentriolar state and after euploid achiasmate meiosis is demonstrated in a model organism (Sections 6.3–6.4, 12.1). Each deep-track node is an established operation in its own field, but their integration is hypothetical and gated; none is assumed.

(c) "Selection may be confounded by cell cycle." Addressed by carrying cell-cycle state as a covariate (adjusted and unadjusted), by cell-cycle scoring, and by a G0/G1-restricted sensitivity analysis (Section 10).

(d) "Human IVG is ethically and legally fraught." The design avoids embryos by construction (Section 13.4) and stages human relevance behind animal validation; where human IVG is legally restricted, the programme's human work is limited to the embryo-free Track A core and T1.

(e) "The safety gate may never pass." We treat a negative safety result as a falsification of the specific track rather than of the programme; the lower-risk tracks (A core, T1) are run first so that the fallback is real rather than rhetorical.

13.9 Minimum dataset required to convert this architecture into a research article

The present manuscript is a protocol/hypothesis paper; the experimental conversion has a defined minimum dataset. The central claim (entropy is a selectable and inducible

property) requires: (i) the coupling map (Objective 1) — single-cell entropy across division history and donor age, n ≥ 20 per group; (ii) proof that the selected fraction is lower-entropy than donor-matched in-vivo HSCs (H2); (iii) a functional engraftment result (H3/H4) against the unselected control; and (iv) a safety-gate result (H5) for the same product. Any one of (ii)–(iv) failing is a falsification of the corresponding hypothesis; the deep-track claims (H4d–H4f) additionally require the node-level results listed in Table 6. The threshold between this paper and its successor is defined here unambiguously. The H1/H2 pilot is specified in Section 5.7; the H3/H4 engraftment protocol is specified in Section 5.5, with the caveat that pilot engraftment power is feasibility-only (Section 2, H3).

14. Conclusions

Ageing of the haematopoietic system is a stem-cell problem, and age-associated single-cell entropy is a computable, cell-intrinsic, selectable property that has never been used as the endpoint of an autologous stem-cell rejuvenation protocol. We formalise a falsifiable research programme whose five tracks — selection/induction (A), reverse-engineered meiotic entropy partition (R), centriole-elimination (C), in-situ niche rejuvenation (T1), and the shared preparation layer (LERR) — are integrated through six shared nodes. Every operation is expressed as a measurable procedure with a defined failure condition, and the safety gate is a co-primary endpoint of every track. The architecture is structured so that negative results surface at the node where evidence is missing, making progress by falsification rather than assertion. If the central coupling holds and the low-entropy state is stable, the programme delivers what no existing approach has: young, safe, autologous adult stem cells, selected and induced by single-cell entropy, returned to the niche without pharmacological immunosuppression, subject to the immunogenicity screen (Section 11).

Declarations

Funding. None to declare for the preprint. The programme is proposed for funding under Horizon Europe EIC Pathfinder Challenges 2026 (Topic: Biotechnology for healthy ageing); this manuscript is the scientific rationale of that proposal.

Competing interests. The author declares no competing interests.

Author self-citations. For transparency, the manuscript cites the author’s own work in four places, all PubMed-indexed and all listed in the reference list with their PMIDs and APA-2005a/2005b disambiguation: Tkemaladze and Chichinadze (2005a), PMID 15886028 (centriole and morphogenetic status, Cell Biology International); Tkemaladze and Chichinadze (2005b), PMID 16336191 (centriolar mechanisms of differentiation and replicative ageing, Biochemistry (Moscow)); Tkemaladze and Chichinadze (2010), PMID

20426623 (centriole, differentiation and senescence, Rejuvenation Research); and Tkemaladze (2023), PMID 36583780 (stem-cell division and centriole accumulation, Molecular Biology Reports). Section 1.5 states that none is independently verified and that the architecture does not depend on any of them being true. No other work by the author is cited.

Ethics. This preprint describes a research programme and hypotheses; it reports no primary data. All future human-cell and animal work will be conducted under the appropriate ethics approvals and cell-therapy regulation.

Data availability. No data were generated for this hypothesis/protocol manuscript. When data are produced, all single-cell data will be deposited in a public repository (e.g., GEO), the analysis code will be released under an open licence, and the pre-registered analysis plan will be made available with the data. The full step-by-step operational protocol is provided as Supplementary Methods / a companion methods document (DOI on registration); the Stage 1 article body contains all decision-relevant parameters needed to evaluate the proposed analyses.

Pre-registration. The hypotheses in Section 2 are submitted for pre-registration before data collection; the registration will be linked from the preprint.

References (APA 7)

Avidor-Reiss, T., & Fishman, E. L. (2019). It takes two (centrioles) to tango. *Reproduction, 157*(2), R33–R51. https://doi.org/10.1530/REP-18-0350 (PMID: 30496124)

Avidor-Reiss, T., Khire, A., Fishman, E. L., & Jo, K. H. (2015). Atypical centrioles during sexual reproduction. *Frontiers in Cell and Developmental Biology, 3*, 21. https://doi.org/10.3389/fcell.2015.00021 (PMID: 25883936)

Bai, L., Li, P., Xiang, Y., Jiao, X., Chen, J., & Song, L. (2024). BRCA1 safeguards genome integrity by activating chromosome asynapsis checkpoint. *Proceedings of the National Academy of Sciences of the United States of America, 121*(19), e2401386121. https://doi.org/10.1073/pnas.2401386121 (PMID: 38696471) Bazzi, H., & Anderson, K. V. (2014). Acentriolar mitosis activates a p53-dependent apoptosis pathway in the mouse embryo. *Proceedings of the National Academy of Sciences of the United States of America, 111*(15), E1491–E1500. https://doi.org/10.1073/pnas.1400568111 (PMID: 24706806)

Bernitz, J. M., Kim, H. S., MacArthur, B., Sieburg, H., & Moore, K. (2016). Hematopoietic stem cells count and remember self-renewal divisions. *Cell, 167*(5), 1296–1309.e10. https://doi.org/10.1016/j.cell.2016.10.022 (PMID: 27839867)

Borrego-Pinto, J., Somogyi, K., Karreman, M. A., König, J., Müller-Reichert, T., Bettencourt-Dias, M., Gönczy, P., Schwab, Y., & Lénárt, P. (2016). Distinct mechanisms eliminate mother and daughter centrioles in meiosis of starfish oocytes. *Journal of Cell Biology, 212*(7), 815–827. https://doi.org/10.1083/jcb.201510083 (PMID: 27002173)

Baltus, A. E., Menke, D. B., Hu, Y.-C., Goodheart, M. L., Carpenter, A. E., de Rooij, D. G., & Page, D. C. (2006). In germ cells of mouse embryonic ovaries, the decision to enter meiosis precedes premeiotic DNA replication. *Nature Genetics, 38*(12), 1430–1434. https://doi.org/10.1038/ng1919 (PMID: 17115059)

Buckley, M. T., Sun, E. D., George, B. M., Liu, L., Schaum, N., Xu, L., Reyes, J. M., Goodell, M. A., Weissman, I. L., Wyss-Coray, T., Rando, T. A., & Brunet, A. (2023). Cell-type-specific aging clocks to quantify aging and rejuvenation in neurogenic regions of the brain. *Nature Aging, 3*(1), 121–137. https://doi.org/10.1038/s43587-022-00335-4 (PMID: 37118510)

Cohen, J. (1988). *Statistical power analysis for the behavioral sciences* (2nd ed.). Lawrence Erlbaum Associates. Conboy, I. M., Conboy, M. J., Wagers, A. J., Girma, E. R., Weissman, I. L., & Rando, T. A. (2005). Rejuvenation of aged progenitor cells by exposure to a young systemic environment. *Nature, 433*(7027), 760–764. https://doi.org/10.1038/nature03260 (PMID: 15716955)

Deuse, T., Hu, X., Agbor-Enoh, S., Koch, M., Spitzer, M. H., Gravina, A., Alawi, M., Marishta, A., Peters, B., Kosaloglu-Yalcin, Z., Yang, Y., … Schrepfer, S. (2019). De novo mutations in mitochondrial DNA of iPSCs produce immunogenic neoepitopes in mice and humans. *Nature Biotechnology, 37*(10), 1137–1144. https://doi.org/10.1038/s41587-019-0227-7 (PMID: 31427818)

Domcke, S., Hill, A. J., Daza, R. M., Cao, J., O'Day, D. R., Pliner, H. A., Aldinger, K. A., Pokholok, D., Zhang, F., Milbank, J. H., Zager, M. A., … Shendure, J. (2020). A human cell atlas of fetal chromatin accessibility. *Science, 370*(6518), eaba7612. https://doi.org/10.1126/science.aba7612 (PMID: 33184180)

Doulatov, S., Vo, L. T., Chou, S. S., Kim, P. G., Arora, N., Li, H., Hadland, B. K., & Bernstein, I. D. (2013). Induction of multipotential hematopoietic progenitors from human pluripotent stem cells via respecification of lineage-restricted precursors. *Cell Stem Cell, 13*(4), 459–470. https://doi.org/10.1016/j.stem.2013.09.002 (PMID: 24094326)

Dussiau, C., Boussaroque, A., Gaillard, M., Bravetti, C., Zaroili, L., Knosp, C., et al. (2022). Hematopoietic differentiation is characterized by a transient peak of entropy at a single cell level. *BMC Biology, 20*(1), 60. https://doi.org/10.1186/s12915-022-01264-9 (PMID: 35260165)

Dykstra, B., Olthof, S., Schreuder, J., Ritsema, M., & de Haan, G. (2011). Clonal analysis reveals multiple functional defects of aged murine hematopoietic stem cells. *Journal of Experimental Medicine, 208*(13), 2691–2703. https://doi.org/10.1084/jem.20111490 (PMID: 22110168)

Edwards, M., Zuccaro, M. V., Sagi, I., Ding, Q., Vershkov, D., Benvenisty, N., Egli, D., & Koren, A. (2021). Delayed DNA replication in haploid human embryonic stem cells. *Genome Research, 31*(12), 2155–2169. https://doi.org/10.1101/gr.275953.121 (PMID: 34810218)

Feng, H., Gao, Y., Jiang, B., Zubair, M., Liu, D., Xu, Z., Wang, Z., Wang, H., Wang, X., Sun, J., Zeng, G., & Huo, L. (2026). ClpP ensures mitochondrial integrity and spermatocyte meiotic progression in mice. *Andrology, 14*(6), 1777–1788. https://doi.org/10.1111/andr.70274 (PMID: 42281331)

Fishman, E. L., Jo, K., Nguyen, Q. P. H., Kong, D., Royfman, R., Cekic, A. R., Khanal, S., Miller, A. L., Simerly, C., Schatten, G., Loncarek, J., & Mennella, V. (2018). A novel atypical sperm centriole is functional during human fertilization. *Nature Communications, 9*(1), 2210. https://doi.org/10.1038/s41467-018-04678-8 (PMID: 29880810)

Goodman, J. M., King, G. A., & Ünal, E. (2020). Cellular quality control during gametogenesis. *Experimental Cell Research, 396*(1), 112247. https://doi.org/10.1016/j.yexcr.2020.112247 (PMID: 32882217)

Hasgur, S., Aryee, K. E., Shultz, L. D., Greiner, D. L., & Brehm, M. A. (2016). Generation of immunodeficient mice bearing human immune systems by the engraftment of hematopoietic stem cells. *Methods in Molecular Biology, 1438*, 67–78. https://doi.org/10.1007/978-1-4939-3661-8_4 (PMID: 27150084)

Hayashi, K., Ogushi, S., Kurimoto, K., Shimamoto, S., Ohta, H., & Saitou, M. (2012). Offspring from oocytes derived from in vitro primordial germ cell-like cells in mice. *Science, 338*(6109), 971–975. https://doi.org/10.1126/science.1226889 (PMID: 23042295)

Hendrickson, P. G., Doráis, J. A., Grow, E. J., Whiddon, J. L., Lim, J.-W., Wike, C. L., Weaver, B. D., Pflueger, C., Emery, B. R., Wilcox, A. L., Nix, D. A., … Cairns, B. R. (2017). Conserved roles of mouse DUX and human DUX4 in activating cleavage-stage genes and MERVL/HERVL retrotransposons. *Nature Genetics, 49*(6), 925–934. https://doi.org/10.1038/ng.3844 (PMID: 28459457)

Howe, K., & FitzHarris, G. (2013). A non-canonical mode of microtubule organization operates throughout pre-implantation development in mouse. *Cell Cycle, 12*(10), 1616–1624. https://doi.org/10.4161/cc.24755 (PMID: 23624836)

Ishiguro, K., Matsuura, K., Tani, N., Takeda, N., Usuki, S., Yamane, M., Sugimoto, M., Fujimura, S., Hosokawa, M., Chuma, S., Ko, M. S. H., & Araki, K. (2020). MEIOSIN directs the switch from mitosis to meiosis in mammalian germ cells. *Developmental Cell, 52*(4), 429–445. https://doi.org/10.1016/j.devcel.2020.01.010 (PMID: 32032549)

Iáñez Picazo, P., Mejía-Ramírez, E., Bari, D., Vitali, E., Florian, M. C., & Petrone, P. (2025). Deep learning predicts haematopoietic stem cell ageing from 3D chromatin images [Preprint]. *bioRxiv*. https://doi.org/10.64898/2025.12.11.693143 (PMID: 41473290)

Ibañez-Solé, O., Ascensión, A. M., Araúzo-Bravo, M. J., & Izeta, A. (2022). Lack of evidence for increased transcriptional noise in aged tissues. *eLife, 11*, e80380. https://doi.org/10.7554/eLife.80380 (PMID: 36576247) Jaiswal, S., Fontanillas, P., Flannick, J., Manning, A., Grauman, P. V., Mar, B. G., Lindsley, R. C., Mermel, C. H., Burtt, N., Chavez, A., Higgins, J. M., … Ebert, B. L. (2014). Age-related clonal hematopoiesis associated with adverse outcomes. *New England Journal of Medicine, 371*(26), 2488–2498. https://doi.org/10.1056/NEJMoa1408617 (PMID: 25426837)

Kawashima, Y., Oda, A., Hikida, Y., & Ohta, K. (2023). Chromosome-dependent aneuploid formation in Spo11-less meiosis. *Genes to Cells, 28*(2), 129–148. https://doi.org/10.1111/gtc.12998 (PMID: 36530025)

Kim, D., & Roy, R. (2006). Cell cycle regulators control centrosome elimination during oogenesis in Caenorhabditis elegans. *Journal of Cell Biology, 174*(6), 751–757. (PMID: 16954347) Kowalczyk, M. S., Tirosh, I., Heckl, D., Rao, T. N., Dixit, A., Haas, B. J., Schneider, R. K., Wagers, A. J., Ebert, B. L., & Regev, A. (2015). Single-cell RNA-seq reveals changes in cell cycle and differentiation programs upon aging of hematopoietic stem cells. *Genome Research, 25*(12), 1860–1872. https://doi.org/10.1101/gr.192237.115 (PMID: 26430063) La Terra, S., English, C. N., Hergert, P., McEwen, B. F., Sluder, G., & Khodjakov, A. (2005). The de novo centriole assembly pathway in HeLa cells: Cell cycle progression and centriole assembly/maturation. *Journal of Cell Biology, 168*(5), 713–722. https://doi.org/10.1083/jcb.200411126 (PMID: 15738265)

Lu, Y., Brommer, B., Tian, X., Krishnan, A., Meer, M., Wang, C., Vera, D. L., Zeng, Q., Yu, D., Bonkowski, M. J., Yang, J.-H., … Sinclair, D. A. (2020). Reprogramming to recover youthful epigenetic information and restore vision. *Nature, 588*(7836), 124–129. https://doi.org/10.1038/s41586-020-2975-4 (PMID: 33268865)

Lv, C., Wang, X., Guo, Y., & Yuan, S. (2020). Role of selective autophagy in spermatogenesis and male fertility. *Cells, 9*(11), 2523. https://doi.org/10.3390/cells9112523 (PMID: 33238415)

Ocampo, A., Reddy, P., Martinez-Redondo, P., Platero-Luengo, A., Hatanaka, F., Hishida, T., Li, M., Lam, D., Kurita, M., Beyret, E., Araoka, T., … Belmonte, J. C. I. (2016). In vivo amelioration of age-associated hallmarks by partial reprogramming. *Cell, 167*(7), 1719–1733. https://doi.org/10.1016/j.cell.2016.11.052 (PMID: 27984723)

Paim, L. M. G., & FitzHarris, G. (2019). Tetraploidy causes chromosomal instability in acentriolar mouse embryos. *Nature Communications, 10*(1), 4834. https://doi.org/10.1038/s41467-019-12772-8 (PMID: 31645568)

Perrier, A., Guiglielmoni, N., Naquin, D., Gorrichon, K., Thermes, C., Lameiras, S., Dammermann, A., Schiffer, P. H., Brunstein, M., Canman, J. C., & Dumont, J. (2024). Maternal inheritance of functional centrioles in two parthenogenetic nematodes. *Nature Communications, 15*(1), 6042. https://doi.org/10.1038/s41467-024-50427-5 (PMID: 39025889)

Pierron, M., Woglar, A., Busso, C., Jha, K., Mikeladze-Dvali, T., Croisier, M., & Gönczy, P. (2023). Centriole elimination during Caenorhabditis elegans oogenesis initiates with loss of the central tube protein SAS-1. *EMBO Journal, 42*(24), e115076. https://doi.org/10.15252/embj.2023115076 (PMID: 37987153)

Pimenta-Marques, A., Bento, I., Lopes, C. A. M., Duarte, P., Jana, S. C., & Bettencourt-Dias, M. (2016). A mechanism for the elimination of the female gamete centrosome in Drosophila melanogaster. *Science, 353*(6294), aaf4866. https://doi.org/10.1126/science.aaf4866 (PMID: 27229142)

Pierson, S. M., Sybirna, A., Wong, F. C. K., & Surani, M. A. (2019). Testing the role of SOX15 in human primordial germ cell fate. *Wellcome Open Research, 4*, 122. https://doi.org/10.12688/wellcomeopenres.15381.2 (PMID: 31583280)

Qiu, J., Papatsenko, D., Niu, X., Schaniel, C., & Moore, K. A. (2014). Divisional history and hematopoietic stem cell function during homeostasis. *Stem Cell Reports, 2*(4), 473–490. https://doi.org/10.1016/j.stemcr.2014.01.016 (PMID: 24749072) Riddell, J., Gazit, R., Garrison, B. S., Guo, G., Saadatpour, A., Mandal, P. K., Ebina, W., Volchkov, P., Yuan, G.-C., Orkin, S. H., & Rossi, D. J. (2014). Reprogramming committed murine blood cells to induced hematopoietic stem cells with defined factors. *Cell, 157*(3), 549–564. https://doi.org/10.1016/j.cell.2014.04.006 (PMID: 24766805) Rinaldi, V. D., Bolcun-Filas, E., Kogo, H., Kurahashi, H., & Schimenti, J. C. (2017). The DNA damage checkpoint eliminates mouse oocytes with chromosome synapsis failure. *Molecular Cell, 67*(6), 1026–1036. https://doi.org/10.1016/j.molcel.2017.07.027 (PMID: 28844861) Rosales-Alvarez, R. E., Rettkowski, J., Herman, J. S., Dumbović, G., Cabezas-Wallscheid, N., & Grün, D. (2023). VarID2 quantifies gene expression noise dynamics and unveils functional heterogeneity of early hematopoietic progenitors. *Genome Biology, 24*(1), 148. https://doi.org/10.1186/s13059-023-02974-1 (PMID: 37353813)

Rossi, D. J., Bryder, D., Zahn, J. M., Ahlenius, H., Sonu, R., Wagers, A. J., & Weissman, I. L. (2005). Cell intrinsic alterations underlie hematopoietic stem cell aging. *Proceedings of the National Academy of Sciences of the United States of America, 102*(26), 9194–9199. https://doi.org/10.1073/pnas.0503280102 (PMID: 15967997)

Sagi, I., Chia, G., Golan-Lev, T., Peretz, M., Weissbein, U., Sui, L., Sauer, M. V., Yanuka, O., Egli, D., & Benvenisty, N. (2016). Derivation and differentiation of haploid human embryonic stem cells. *Nature, 532*(7597), 107–111. https://doi.org/10.1038/nature17408 (PMID: 26982723)

Sahu, S. K., Reddy, P., Lu, J., Shao, Y., Wang, C. T., Tsuji, M., Delicado, E. N., Rodriguez, E. C., & Izpisua Belmonte, J. C. (2024). Targeted partial reprogramming of age-associated cell states improves markers of health in mouse models of aging. *Science Translational Medicine, 16*(764), eadg1777. https://doi.org/10.1126/scitranslmed.adg1777 (PMID: 39259812)

Samaddar, M., Goudeau, J., Sanchez, M., Hall, D. H., Bohnert, K. A., Ingaramo, M., & Kenyon, C. (2021). A genetic screen identifies new steps in oocyte maturation that enhance proteostasis in the immortal germ lineage. *eLife, 10*, e62653. https://doi.org/10.7554/eLife.62653 (PMID: 33848238)

Schneider, I., de Ruijter-Villani, M., Hossain, M. J., Stout, T. A. E., & Ellenberg, J. (2021). Dual spindles assemble in bovine zygotes despite the presence of paternal centrosomes. *Journal of Cell Biology, 220*(11), e202010106. https://doi.org/10.1083/jcb.202010106 (PMID: 34550316)

Schuh, M., & Ellenberg, J. (2007). Self-organization of MTOCs replaces centrosome function during acentrosomal spindle assembly in live mouse oocytes. *Cell, 130*(3), 484–498. https://doi.org/10.1016/j.cell.2007.06.025 (PMID: 17693257)

Shamseer, L., Moher, D., Clarke, M., Ghersi, D., Liberati, A., Petticrew, M., Shekelle, P., & Stewart, L. A. (2015). Preferred reporting items for systematic review and meta-analysis protocols (PRISMA-P) 2015: Elaboration and explanation. *Systematic Reviews, 4*, 1. https://doi.org/10.1186/2046-4053-4-1 (PMID: 25554246)

So, C., Seres, K. B., Steyer, A. M., Mönnich, E., Clift, D., Pejkovska, A., Möbius, W., & Schuh, M. (2019). A liquid-like spindle domain promotes acentrosomal spindle assembly in mammalian oocytes. *Science, 364*(6447), eaat9557. https://doi.org/10.1126/science.aat9557 (PMID: 31249032)

Stevens, N. R., Raposo, A. A. S. F., Basto, R., St Johnston, D., & Raff, J. W. (2007). From stem cell to embryo without centrioles. *Current Biology, 17*(17), 1498–1503. https://doi.org/10.1016/j.cub.2007.07.060 (PMID: 17716897)

Stevens, H., Yücel, A., Gould, R., Cai, G., Gladyshev, V. N., & Plesa, A. (2026). Architectural fragility of gene regulatory networks underlies hematopoietic stem cell aging [Preprint]. *bioRxiv*. https://doi.org/10.64898/2026.06.03.729976 (PMID: 42282599) Sugimura, R., Jha, D. K., Han, A., Soria-Valles, C., da Rocha, E. L., Lu, Y.-F., Goettel, J. A., Serrao, E., Rowe, R. G., Malleshaiah, M., Underwood, I., & Daley, G. Q. (2017). Haematopoietic stem and progenitor cells from human pluripotent stem cells. *Nature, 545*(7655), 432–438. https://doi.org/10.1038/nature22370 (PMID: 28514439) Takahashi, K., & Yamanaka, S. (2006). Induction of pluripotent stem cells from mouse embryonic and adult fibroblast cultures by defined factors. *Cell, 126*(4), 663–676. https://doi.org/10.1016/j.cell.2006.07.024 (PMID: 16904174)

Teschendorff, A. E., & Enver, T. (2017). Single-cell entropy for accurate estimation of differentiation potency from a cell's transcriptome. *Nature Communications, 8*, 15599. https://doi.org/10.1038/ncomms15599 (PMID: 28569836)

Teschendorff, A. E., Sollich, P., & Kuehn, R. (2014). Signalling entropy: A novel network-theoretical framework for systems analysis and interpretation of functional omic data. *Methods, 67*(3), 282–293. https://doi.org/10.1016/j.ymeth.2014.03.013 (PMID: 24675401) Tkemaladze, J. (2023). Reduction, proliferation, and differentiation defects of stem cells over time: A consequence of selective accumulation of old centrioles in the stem cells? *Molecular Biology Reports, 50*(3), 2751–2761. https://doi.org/10.1007/s11033-022-08203-5 (PMID: 36583780)

Tkemaladze, J., & Chichinadze, K. (2005a). Potential role of centrioles in determining the morphogenetic status of animal somatic cells. *Cell Biology International, 29*(5), 370–374. https://doi.org/10.1016/j.cellbi.2005.03.003 (PMID: 15886028)

Tkemaladze, J., & Chichinadze, K. (2005b). Centriolar mechanisms of differentiation and replicative aging of higher animal cells. *Biochemistry (Moscow), 70*(11), 1288–1303. https://doi.org/10.1007/s10541-005-0261-6 (PMID: 16336191)

Tkemaladze, J., & Chichinadze, K. (2010). Centriole, differentiation, and senescence. *Rejuvenation Research, 13*(2–3), 261–262. https://doi.org/10.1089/rej.2009.0904 (PMID: 20426623)

Uetake, Y., Loncarek, J., Nordberg, J. J., English, C. N., La Terra, S., Khodjakov, A., & Sluder, G. (2007). Cell cycle progression and de novo centriole assembly after centrosomal removal in untransformed human cells. *Journal of Cell Biology, 176*(2), 173–182. https://doi.org/10.1083/jcb.200607073 (PMID: 17227892)

Uzbekov, R., Singina, G., Shedova, E., Banliat, C., Avidor-Reiss, T., & Uzbekova, S. (2023). Centrosome formation in the bovine early embryo. *Cells, 12*(9), 1335. https://doi.org/10.3390/cells12091335 (PMID: 37174735)

Valenzuela-Villatoro, M., de la Cuesta, P. L., Guerrero-Gómez, D., Gómez-Orte, E., Schiavi, A., Maglioni, S., Montero, M., Fonteriz, R., Casas-Martínez, J., Briand, N., Xu, J., … Miranda-Vizuete, A. (2026). Mitochondrial redox homeostasis links organellar stress surveillance to germline and somatic integrity in Caenorhabditis elegans. *Redox Biology, 93*, 104115. https://doi.org/10.1016/j.redox.2026.104115 (PMID: 41996933)

Warren, L., Manos, P. D., Ahfeldt, T., Loh, Y.-H., Li, H., Lau, F., Ebina, W., Mandal, P. K., Smith, Z. D., Meissner, A., Daley, G. Q., … Rossi, D. J. (2010). Highly efficient reprogramming to pluripotency and directed differentiation of human cells with synthetic modified mRNA. *Cell Stem Cell,* 7(5), 618–630. https://doi.org/10.1016/j.stem.2010.08.012 (PMID: 20888316)

Wong, Y. L., Anzola, J. V., Davis, R. L., Yoon, M., Motamedi, A., Kroll, A., Seo, C. P., Hsia, J. E., Kim, S. K., Mitchell, J. W., Mitchell, B. J., & Desai, A. (2015). Cell biology: Reversible centriole depletion with an inhibitor of Polo-like kinase 4. *Science, 348*(6239), 1155–1160. https://doi.org/10.1126/science.aaa5111 (PMID: 25931445)

Xu, M., Pirtskhalava, T., Farr, J. N., Weigand, B. M., Palmer, A. K., Weivoda, M. M., Inman, C. L., Ogrodnik, M. B., Hachfeld, C. M., Fraser, D. G., Onken, J. L., … Kirkland, J. L. (2018). Senolytics improve physical function and increase lifespan in old age. *Nature Medicine, 24*(8), 1246–1256. https://doi.org/10.1038/s41591-018-0092-9 (PMID: 29988130)

Xu, X., Zhang, Y., Cheng, H., & Zhou, R. (2021). SPATA33 functions as a mitophagy receptor in mammalian germline. *Autophagy, 17*(5), 1284–1286. https://doi.org/10.1080/15548627.2021.1909836 (PMID: 33818286)

Yang, Y., Hess, P. R., Huang, S., Teneche, M. G., Wang, H., Miller, K. N., Davis, A. E., Miciano, C., Li, K. Y., Mamde, S., Yip, K., … Zhang, N. R. (2026). A manifold-based measure of transcriptional entropy for quantifying aging in single cells [Preprint]. *bioRxiv*. https://doi.org/10.64898/2026.01.24.701460 (PMID: 41648477)

Zhang, H., Chen, Y., Jiang, J., Ding, Y., Hu, S., Zhou, Z., & Chen, L. (2026). Mitochondrial microautophagy: An emerging pathway in maintaining mitochondrial homeostasis. *Antioxidants & Redox Signaling*. Advance online publication. https://doi.org/10.1177/15230864261481794 (PMID: 42686641)

Appendix A. Systematic search strategy

Searches were run against PubMed (E-utilities, esearch/esummary) on 2026-09-20 and re-run on 2026-10-02. Key queries and result counts:

Query	Hits

Query	Hits
`single-cell entropy AND stem cell AND rejuvenation`	0
`entropy AND autologous AND hematopoietic stem cell AND selection`	1 (unrelated)
`division rate AND single-cell entropy`	2 (unrelated)
`entropy AND haematopoietic differentiation`	1 (Dussiau et al., 2022 — transient entropy peak across haematopoietic differentiation at single-cell level; differentiation-potency entropy, distinct from the age-associated selection use here)
`signaling entropy AND stem cell aging`	1 (non-target)
`centriole transplant AND cell fate`	0
`reprogramming AND entropy AND rejuvenation`	4 (non-target)
`chromatin entropy HSC ageing` (preprints)	1 (Iáñez Picazo et al., 2025 — chromatin entropy as a predictive marker of HSC ageing; distinct from the transcriptomic age-associated entropy used here)
`manifold transcriptional entropy aging` (preprints)	1 (Yang et al., 2026 — conceptual neighbourhood active; confirms age-associated entropy rises with age and mitotic age)
`architectural fragility gene regulatory networks HSC` (preprints)	1 (Stevens et al., 2026 — descriptive multi-omics atlas, > 380,000 paired RNA/ATAC profiles, 77 donors; cis-regulatory entropy rises with age; juxtaposed with the operational use here in Section 1.3)
`autologous iPSC mitochondrial neoantigens`	1 (Deuse et al., 2019 — autologous iPSC-derived products are not inherently immunologically inert)

Search-boundary note: the 0-hit queries in the table are acknowledged as narrow; broader terms (e.g., *transcriptional entropy AND stem cell AND aging*), a Web of Science/Scopus/Embase search, and a PRISMA-S flow diagram accompany the Stage 2 experimental paper.

Interpretation. No published study uses *transcriptomic* age-associated single-cell entropy as a selectable and inducible property for autologous niche-replacement; the conceptual neighbourhood is active (Yang et al., 2026; Iáñez Picazo et al., 2025). The novelty claim (Section 1.3) is stated at this precise level, distinguishing transcriptomic age-associated entropy from the chromatin-entropy predictive marker work. An earlier version of this manuscript overstated the claim as “no hits at all”; the corrected reading is that the neighbourhood is populated but the specific integrated operation (select by transcriptomic age-associated entropy, return to niche, test function) is untested. This appendix is a scoping search and is labelled as such; the databases covered at this stage are PubMed (E-utilities) and the bioRxiv/medRxiv preprint servers, with inclusion and exclusion criteria and full query strings archived with the Stage 1 registration. A PRISMA-S-compliant search across Web of Science, Scopus, and Embase, with a flow diagram, will accompany the experimental paper (Stage 2). Protocol reporting for the Stage 1 plan follows the PRISMA-P 2015 statement (Shamseer et al., 2015), including the planned inclusion/exclusion criteria and data items. Because two of the key method citations (Yang et al., 2026; Iáñez Picazo et al., 2025) are preprints, they are graded [I]/[H] in Table 3 rather than [E], and are cited with their preprint identifiers.